

ARTICLE

Tumor cell-intrinsic Piezo2 drives radioresistance by impairing CD8⁺ T cell stemness maintenance

Naijun Miao^{1,2}*, Dongqing Cao²*, Jingsi Jin²*, Guizhi Ma^{1,2}, Haihui Yu³, Junwen Qu⁴, Guiping Li⁵, Caixia Gao¹, Dong Dong⁶, Fan Xia⁷, and Wenwen Li^{1,2}

Changes in mechanosensitive ion channels following radiation have seldom been linked to therapeutic sensitivity or specific factors involved in antitumor immunity. Here, in this study, we found that the mechanical force sensor, Piezo2, was significantly upregulated in tumor cells after radiation, and Piezo2 knockout in tumor cells enhanced tumor growth suppression by radiotherapy. Specifically, loss of Piezo2 in tumor cells induced their IL-15 expression via unleashing JAK2/ STAT1/IRF-1 axis after radiation. This increase in IL-15 activates IL-15Rα on tumor-infiltrating CD8⁺ T cells, thereby leading to their augmented effector and stem cell-like properties, along with reduced terminal exhausted feature. Importantly, Piezo2 expression was negatively correlated with CD8 infiltration, as well as with radiosensitivity of patients with rectum adenocarcinoma receiving radiotherapy treatment. Together, our findings reveal that tumor cell-intrinsic Piezo2 induces radioresistance by dampening the IRF-1/IL-15 axis, thus leading to impaired CD8⁺ T cell-dependent antitumor responses, providing insights into the further development of combination strategies to treat radioresistant cancers.

Introduction

Radiotherapy is a widely used and often effective treatment for a variety of cancers. Radiation stimulates antitumor immunity by promoting the release of tumor antigens, chemokines, and cytokines, subsequently increasing the capacity for cross-presentation in antigen-presenting cells (APCs) and enhancing the function of cytotoxic CD8⁺ T cells (Gajewski et al., 2013; Herrera et al., 2017; McLaughlin et al., 2020). However, many patients show poor response to radiotherapy and frequently experience tumor recurrence due to the immunosuppressive effects of some tumor-intrinsic or tumor-extrinsic factors that drive tumor immune evasion (Liang et al., 2017; Kalbasi et al., 2017; Mondini et al., 2019). Reliable strategies for augmenting radiation-mediated antitumor immunity are therefore essential to improving response in these patients.

Mechanosensitive ion channels play an important role in converting mechanical stimuli into electrical or chemical signals (Coste et al., 2010). Among the well-studied mechanosensitive ion channels, Piezo2 has been implicated in a range of physiological processes, including blood pressure regulation, lung stretch sensing, and urination, among others (Coste et al., 2010; Szczot et al., 2021). Increasing evidence supports a strong link between Piezo2 function and tumor development, progression,

and invasion (Lou et al., 2019; Liu et al., 2022; Chen et al., 2023). However, whether changes in such membrane-associated mechanical stress sensors after radiation could also affect antitumor response remains largely unknown.

Radiation-induced cytokine release plays a major role in antitumor efficacy and is associated with tissue damage and inflammation resulting from radiotherapy (Christensen et al., 2009; Palata et al., 2019). Interleukin 15 (IL-15), the cognate ligand of IL-15 receptor-α (IL-15Rα), promotes IgG secretion from B cells and participates in regulating self-renewal, expansion, and multipotency in stem cell-like CD8⁺ T cells. Furthermore, IL-15 is a major cytokine that has been identified to date as positively correlated with antitumor immune cell infiltration and progression-free survival in colorectal cancer patients (Mlecnik et al., 2014). In another study, radiotherapy combined with IL-15 treatment was found to result in loss of CD8⁺ T cell tolerance in response to lymphopenia (Oelert et al., 2010). However, relatively little is known about whether and how IL-15 can improve the antitumor efficacy of radiotherapy.

In this work, we found that Piezo2 expression was significantly increased in tumor cells after radiation, which subsequently

¹Precision Research Center for Refractory Diseases, Shanghai General Hospital, Shanghai Jiao Tong University School of Medicine, Shanghai, China; ²Department of Immunology and Microbiology, Shanghai Institute of Immunology, Shanghai Jiao Tong University School of Medicine, Shanghai, China; ³School of Basic Medical Sciences, Shanghai Jiao Tong University School of Medicine, Shanghai, China; ⁴Department of Urology, Renji Hospital, Shanghai Jiao Tong University School of Medicine, Shanghai, China; ⁵Core Facility of Basic Medical Sciences, Shanghai Jiao Tong University School of Medicine, Shanghai, China; ⁷Department of Radiation Oncology, Fudan University Shanghai Cancer Center, Shanghai, China.

*N.J. Miao, D.Q. Cao, and J.S. Jin contributed equally to this paper. Correspondence to Wenwen Li: wenwenli2016@sjtu.edu.cn; Fan Xia: tcxiafan@hotmail.com.

© 2024 Miao et al. This article is distributed under the terms of an Attribution–Noncommercial–Share Alike–No Mirror Sites license for the first six months after the publication date (see http://www.rupress.org/terms/). After six months it is available under a Creative Commons License (Attribution–Noncommercial–Share Alike 4.0 International license, as described at https://creativecommons.org/licenses/by-nc-sa/4.0/).





suppressed their IL-15 production via phospho-JAK2/STAT1-IRF-1 pathway inhibition, consequently resulting in loss of stemness in tumor-infiltrating CD8+ T cells. Findings in the current study illustrate a previously unrecognized radiation-responsive role of Piezo2 in promoting radioresistance by suppressing IL-15 release in tumor cells and suggests the further exploration of Piezo2-based targeting as a supplementary strategy to improve response to radiotherapy.

Results

Piezo2 knockout (KO) enhances antitumor effects of radiotherapy

While screening for the effects of radiation on phenotype in the radio-sensitive MC38 (murine colon adenocarcinoma) cell line, we observed that cells appeared generally larger following radiation. The quantification by scanning electron microscopy and immunofluorescence staining of the cytoskeleton verified that cell size indeed increased following radiation in MC38 (Fig. 1 A and Fig. S1 A) and radio-resistant B16F1 murine melanoma cells (Fig. S1 B). In addition, flow cytometry analysis of MC38tdTomato+ cells isolated from tumor-bearing WT mice further confirmed the post-radiation increase in size on days 3 and 6 after radiation (Fig. S1, C and D). Given that mechanical force sensors may change along with cell size and cytoskeleton stretch (Satir and Christensen, 2007; Davis et al., 2023; Jin et al., 2020), we therefore performed RNA sequencing (RNA-seq) in irradiated and non-irradiated MC38 cells to identify related genes. Gene Ontology (GO) term analysis showed that the genes involved in the regulation of membrane potential were enriched in irradiated MC38 cells (Fig. 1 B). Moreover, gene set enrichment analysis (GSEA) further indicated that differentially expressed genes (DEGs) involved in the cellular response to abiotic stimulus were also enriched in irradiated MC38 cells (Fig. 1 C). We further analyzed the common mechanosensitive ion channels (Piezo2, Trpv2, Trpv6, Kcnk2, Kcnk4, Kcnk5, Kcnk6, and Kcnk7). Based on the obvious upregulation of Piezo2 in response to radiation (Fig. 1 D), we then focused on the possible role of Piezo2 in irradiation-induced tumor response. Consistent with RNAseq data, quantitative PCR (Q-PCR) analysis (Fig. 1 E) and western blots (Fig. S1, E and F) confirmed that Piezo2 was upregulated in irradiated MC38 and B16F1 tumor cells compared with its expression in non-irradiated controls. We also observed the increase of Piezo2 expression either on the surface or in the cytosol of sorted tdTomato+ cells from tumors (Fig. 1 F). In addition, as a sensory transduction channel, Piezo2 permits Ca2+ passage after the mechanical force on the cell membrane (McHugh et al., 2010). We next determined the effect of radiation on Ca²⁺ uptake. The results showed that Ca²⁺ concentration was increased in WT tumor cells after radiation treatment compared with that in non-irradiated WT cells (Fig. S1 G).

To investigate the function of Piezo2 in tumor sensitivity to irradiation, we used CRISPR-Cas9 genome editing with different guide RNAs to generate MC38 and B16F1 cell lines with Piezo2 deletion. After confirming that Piezo2 expression was remarkably decreased in the Piezo2 KO cell lines compared with that in the corresponding WT CRISPR-Ctrl lines (Fig. S1 H), we assessed

whether Piezo2 deficiency affects cell growth. The determination of cell viability illustrated that loss of Piezo2 had no impact on cell proliferation in MC38 and B16F1 cells (Fig. S1 I). Then, Piezo2 KO and WT MC38 and B16F1 cell lines were each respectively used to establish subcutaneous tumors in the right flank of C57BL/6 mice. Monitoring tumor growth after local radiation treatment indicated that tumor volume was markedly lower after radiation in Piezo2 KO MC38 tumors compared with that of WT tumors (Fig. 1 G) and with a similar pronounced effect in Piezo2 KO B16F1 tumors (Fig. 1 H). These results suggested that loss of Piezo2 could enhance the antitumor effects of radiation.

Radiation has been shown to confer abscopal effects in several types of human cancers and is closely linked to the host immune response (Herrera et al., 2017). We therefore next investigated whether Piezo2 in primary tumors contributed to the abscopal effects of local radiation in untreated secondary tumors. Comparison of tumor volumes after radiation showed that WT secondary tumors corresponding to irradiated primary Piezo2 KO tumors showed greater inhibition of growth than WT secondary tumors related to irradiated primary WT tumors (Fig. 1 I). These data implied that Piezo2 in primary tumor cells could restrict the growth of unirradiated secondary tumors, potentially via induction of antitumor immune adaptive response.

Piezo2 deficiency in tumor cells enhances the function and stemness of intratumoral CD8⁺ T cells after radiation

Previous studies have shown that adaptive immune CD8+T cells, which are cytotoxic to tumor cells, are required for postradiation tumor control (Herrera et al., 2017; McLaughlin et al., 2020; Arina et al., 2020). In agreement with previous studies (Gupta et al., 2012; Rodriguez-Ruiz et al., 2016; Lee et al., 2009), the antitumor effect of radiation was reduced after the administration of depletion antibodies against CD8+ T cells in WT tumors (Fig. 2 A). Furthermore, the enhancement of tumor growth suppression in irradiated Piezo2 KO tumors was also reversed after CD8+ T cell depletion, which indicated that adaptive immune responses played an essential role in Piezo2 deficiencymediated reinforced antitumor effect of radiation (Fig. 2 A). To assess whether Piezo2 in tumor cells plays a role in recruiting CD8⁺ T cells, we analyzed the proportion of CD8⁺ T cells in the tumor microenvironment (TME) using flow cytometry on days 7 and 14 after radiation. We found that the percentage of CD8+ T cells was greater in irradiated Piezo2-/- tumors compared with that in irradiated WT tumors (Fig. 2 B). Moreover, staining for intracellular cytokines showed that loss of Piezo2 resulted in enrichment with IFN- γ ⁺TNF- α ⁺CD8⁺ T cells (Fig. 2 C), which was further supported by our observation of increased IFN-y production in irradiated cells (Fig. 2 D).

Stem cell-like T cells are critical for a durable antitumor response. These subpopulations characteristically exhibit self-renewal, expansion, and pluripotency, and are identified by the expression of TCF-1 (encoded by Tcf7 gene) and Ki-67 (Siddiqui et al., 2019; Li et al., 2020; Prokhnevska et al., 2023). To determine whether the enhanced accumulation of CD8+T cells was due to increased proliferative potential after radiation, we analyzed Ki-67+, TCF-1+, and CD62L+ cells within the



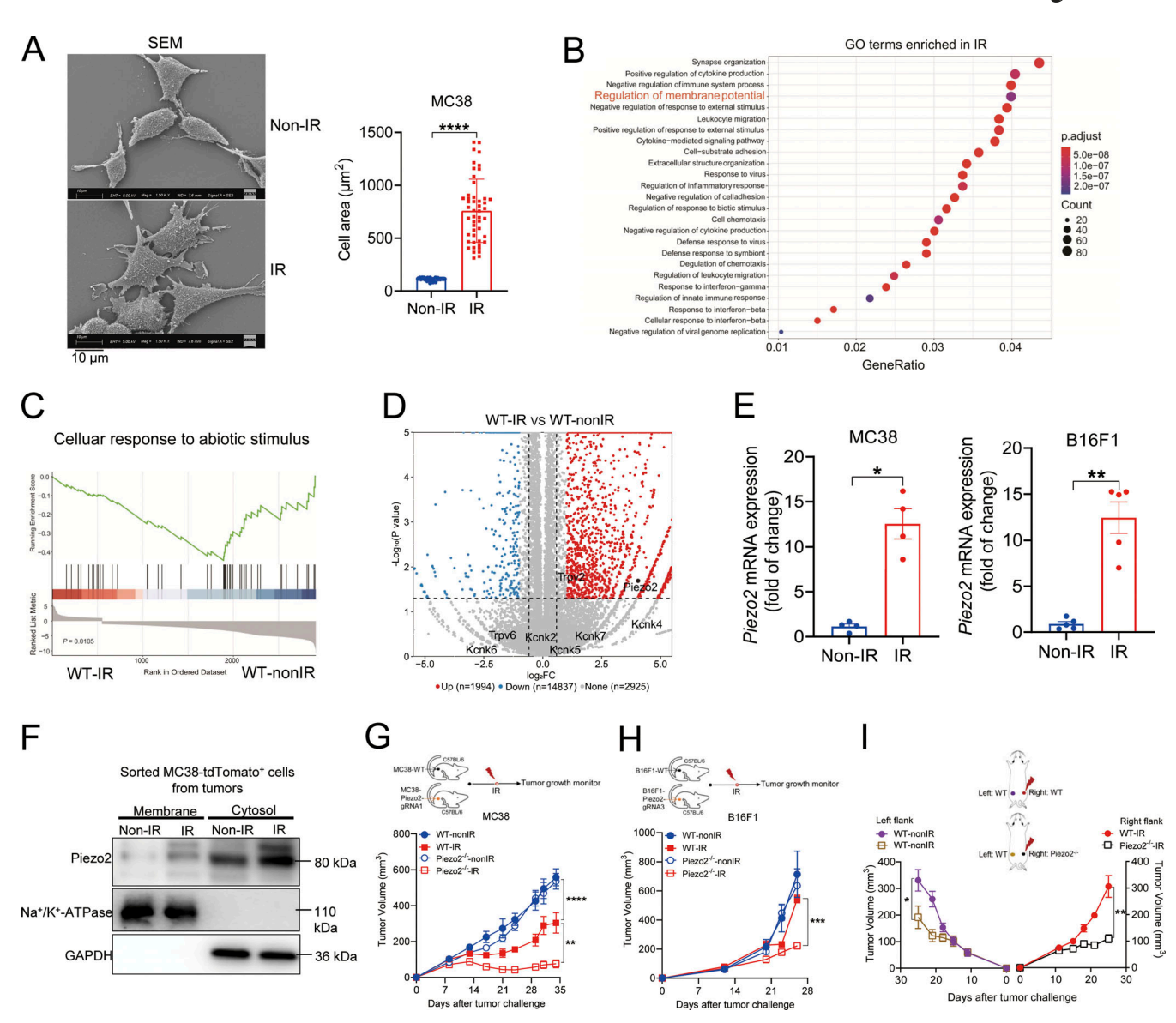


Figure 1. **Effects of Piezo2 KO on tumor response to radiation. (A)** Scanning electron microscope (SEM) showing the size of MC38 cells with one fraction of 30 Gy IR or without IR (left; scale bar = $10 \mu m$), and the quantification of cell size (right). **(B–D)** MC38 cells were irradiated at a single fraction of 30 Gy. At 60 h after radiation, total RNA was extracted and further analyzed by RNA-seq. GO enrichment analysis of membrane potential signaling pathway (B), GSEA of cellular response to abiotic stimulus (C), and volcano plot exhibiting the DEGs of mechanosensitive ion channels from RNA-seq data (D). **(E)** The *Piezo2* mRNA expression in MC38 and B16F1 cells after IR treatment was shown from three independent experiments. **(F)** Piezo2 expression was determined on the surface or in the cytosol of CD45⁻tdTomato⁺ tumor cells sorted from WT MC38 tumors on day 5 after IR treatment. Representative data were shown from one independent experiment using pooled tdTomato⁺ tumor cells from tumors (n = 6 mice per group). **(G)** Mice were subcutaneously inoculated with WT MC38 and Piezo2^{-/-} MC38 tumor cells, and then established tumors were treated locally with one fraction of 18-Gy IR. The tumor growth curve was represented from two independent experiments (n = 6-8 mice per group). **(H)** Mice were subcutaneously inoculated with WT B16F1 and Piezo2^{-/-} B16F1 tumor cells, and then established tumors were treated locally with one fraction of 18-Gy IR. The tumor growth curve was represented from two independent experiments (n = 3-4 mice per group). **(I)** The tumor growth curve of unirradiated secondary tumors (WT MC38, left flank) and irradiated primary tumors (WT MC38 or Piezo2^{-/-} MC38, right flank) in C57BL/6 mice was represented from two independent experiments (n = 5-6 mice per group). Data were represented as means ± SEM. The comparisons of two nonparametric datasets in A and E were calculated by the Mann–Whitney U test. G–I were analyzed by one-way ANOVA with multiple comparison tests. *P < 0.05;

intratumoral PD-1*CD44*TIM3^{low}CD8* T cell subpopulation by flow cytometry. We observed that the proportions of cells expressing the Ki-67, TCF-1, or CD62L stemness markers all increased among tumor-infiltrating PD-1*CD44*TIM3^{low}CD8* T cells in Piezo2 KO tumors compared with that in WT MC38 tumors on days 7 (Fig. 2, E-G) and 14 (Fig. S2, A-C) after radiation treatment. Moreover, examination of the T cell exhaustion

marker, TOX, revealed that the proportion of TOX^+ in PD-1+CD44+TIM3lowCD8+ T cells was reduced in irradiated Piezo2 KO tumors compared with that in WT tumors on days 7 and 14 after radiation (Fig. 2 H and Fig. S2 D). In addition, flow cytometry quantification of CD8+ T cells revealed that Piezo2-/-tumors receiving radiation had a lower proportion of PD-1+CD8+ T cells (Fig. 2 I and Fig. S2 E), but increased Slamf6 expression



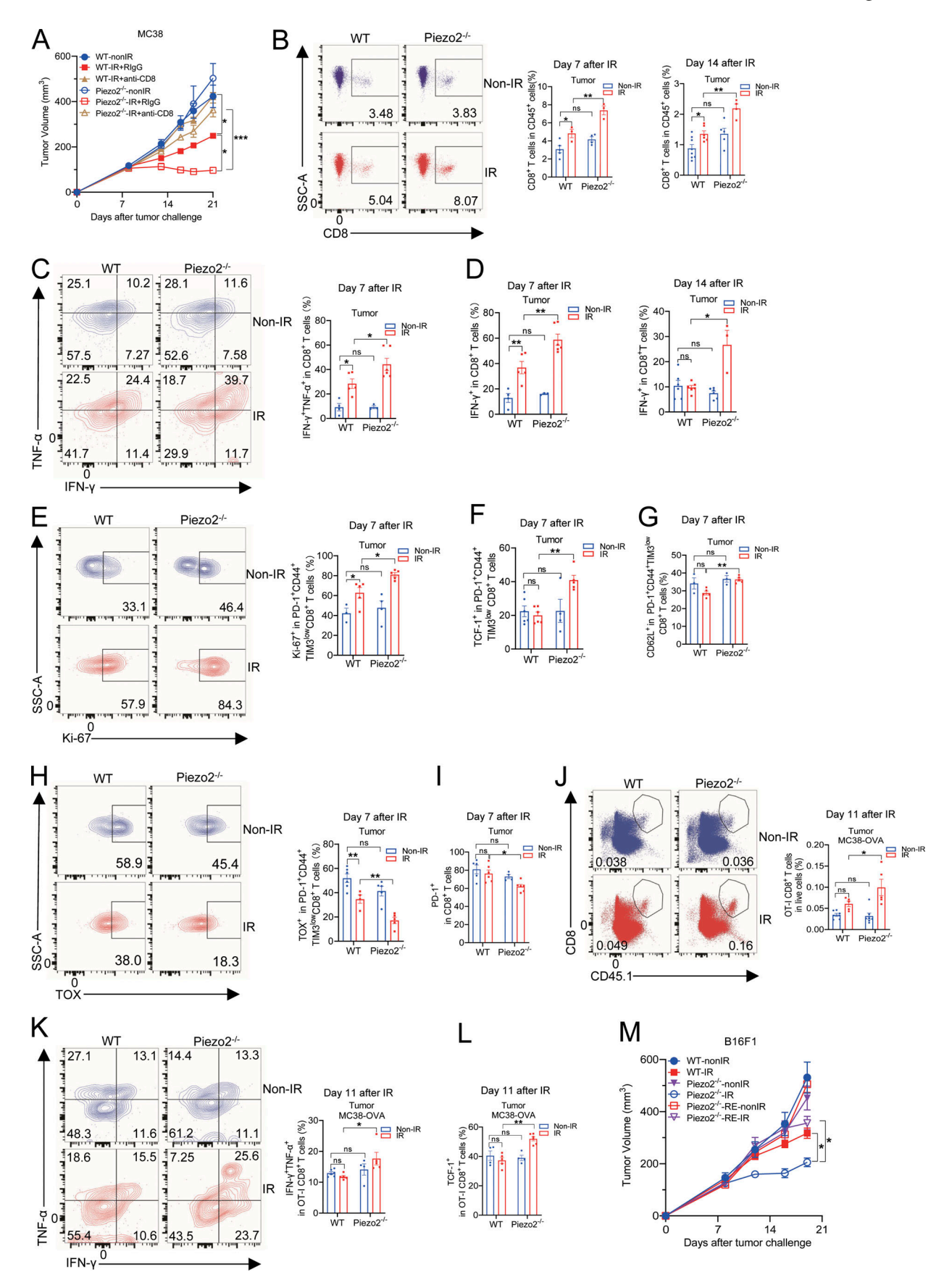


Figure 2. **Effects of Piezo2 KO on intratumoral CD8**⁺ **T cell function and stemness after radiation. (A–I)** Mice were transplanted subcutaneously with 2 × 10⁶ MC38 cells and then established tumors were treated locally with one fraction of 18-Gy IR. **(A)** To deplete CD8⁺ T cells, mice were injected with anti-CD8



antibody (200 µg per mouse, intraperitoneally (i.p.) starting on the day receiving IR treatment, every 2 days for a total of three times), RIgG, rat IgG. The tumor growth curve of WT and Piezo2-/- MC38 tumors in C57BL/6 mice with or without anti-CD8 treatment after IR was represented from two independent experiments (n = 4-6 mice per group). (B) Representative data and quantification of the percentage of CD8+T cells in CD45+ cells from WT and Piezo2-/- MC38 tumors on days 7 and 14 after IR treatment were shown from three independent experiments (n = 3-8 mice per group). (C) Representative data and quantification of the percentage of IFN-γ+TNF-α+CD8+ T cells from WT and Piezo2^{-/-} MC38 tumors on day 7 after IR were shown from three independent experiments (n = 3-6 mice per group). (D) Quantitation of the percentage of IFN- γ ⁺CD8⁺ T cells from WT and Piezo2^{-/-} MC38 tumors on days 7 and 14 after IR was shown from three independent experiments (n = 3-6 mice per group). (**E-H**) Representative data and quantification of the percentage of Ki-67⁺ (E), TCF-1⁺ (F), CD62L+ (G), and TOX+ (H) in PD-1+CD44+TIM3low CD8+ T cells from WT and Piezo2-/- MC38 tumors on day 7 after IR are shown from three independent experiments (n = 3-6 mice per group). (1) Quantification of the percentage of PD-1⁺ in CD8⁺ T cells from WT and Piezo2^{-/-} MC38 tumors on day 7 after IR was shown from three independent experiments (n = 4-6 mice per group). (J and K) Mice were transplanted subcutaneously with 2×10^6 MC38-OVA cells, and then established tumors were treated locally with one fraction of 18-Gy IR. On the next day of receiving radiation treatment, 2 × 10⁶ activated OT-I CD8+ T cells were adoptively transferred into mice via retroorbital intravenous injection. Representative data and quantification of the percentage of OT-I CD8+ T cells (J), and IFN- γ^+ TNF- α^+ (K) in OT-I CD8+ T cells from WT and Piezo2-/- MC38 tumors on day 11 after IR were shown from two independent experiments (J, n=5-7 mice per group; K, n = 4-6 mice per group). (L) Quantification of the percentage of TCF-1+ in OT-I CD8+ T cells from WT and Piezo2-/- MC38 tumors on day 11 after IR was shown from two independent experiments (n = 4-5 mice per group). (M) Mice were transplanted subcutaneously with 1×10^6 cells WT, Piezo $2^{-/-}$, and Piezo^{2-/-}-RE B16F1 cells, and then established tumors were treated locally with one fraction of 18-Gy IR. The tumor growth curve was represented from two independent experiments (n = 4-6 mice per group). Data were represented as means \pm SEM. A and M were analyzed by two-way ANOVA with multiple comparison tests; B-L were performed by one-way ANOVA with multiple comparison tests. *P < 0.05; **P < 0.01, ***P < 0.001, ns, no significant difference.

(T cell stemness surface marker) on CD8 $^+$ T cells compared with WT control tumors on days 7 and 14 following radiation (Fig. S2, F and G).

Further examination of subpopulations within draining lymph nodes (DLNs) of Piezo2^{-/-} tumor-bearing mice showed that CD8⁺ T cells were more abundant than in DLNs of mice with WT tumors following irradiation (Fig. S2 H). Moreover, CD8⁺ T cells in DLNs of Piezo2 KO tumor-bearing mice exhibited greater enrichment of subsets expressing function markers than those in WT tumor-bearing mice (Fig. S2, I and J). By contrast, CD8⁺ T cells from DLNs of Piezo2^{-/-} tumor-bearing mice showed no obvious increase in Ki-67 expression levels or percentage of TCF-1⁺ cells (Fig. S2, K and L).

We next investigated the effects of Piezo2 deficiency on antigen-specific CD8+ T cells within irradiated tumors. We applied CRISPR-Cas9 genome editing with guide RNAs to generate Piezo2^{-/-} MC38-OVA cell line and determined the knockdown efficiency of Piezo2 expression by western blot (Fig. S2 M). After the establishment of tumors, we adoptively transferred OVAspecific CD45.1+ OT-I T cells to MC38-OVA-bearing mice on the next day of receiving radiation treatment. Our result indicated that the infiltration of OT-I CD8+ T cells was greater in irradiated Piezo2-/- tumors compared with that in irradiated WT tumors (Fig. 2 J). Moreover, the results of staining for intracellular cytokines suggested that loss of Piezo2 contributed to the enrichment of IFN- γ^+ TNF- α^+ OT-I CD8+ T cells (Fig. 2 K). Furthermore, the proportions of cells expressing TCF-1 increased among tumor-infiltrating OT-I CD8+ T cells in Piezo2 KO tumors compared with that in WT MC38 tumors after radiation treatment (Fig. 2 L). We next explored whether the re-expression of Piezo2 in Piezo2 KO cells could reverse the augmented tumor growth suppression in irradiated Piezo2-/tumors. Piezo2 expression was determined in Piezo2-/- and reexpressed (Piezo2-/--RE) cells by western blot (Fig. S2 N). In addition, Ca²⁺ concentration was increased in CD45⁻ cells from irradiated Piezo2^{-/-}-RE tumors compared with that in Piezo2^{-/-} tumors after radiation (Fig. S2 O). By monitoring tumor growth, we observed that the enhanced antitumor effect of Piezo2 KO in irradiated tumors was diminished in Piezo2-re-expressed tumors

receiving radiation treatment (Fig. 2 M). Through further analysis, we assessed the effects of Piezo2 re-expression on the regulation of tumor-infiltrating CD8+ T cells within Piezo2-/-tumors. In agreement with our former results, the infiltration of CD8+ T cells and the frequency of IFN- γ + cells detected among CD8+ T cells was higher in irradiated Piezo2 KO tumors but decreased after re-expressing Piezo2 (Fig. S2, P and Q). Furthermore, the frequency of TOX+ in exhausted CD8+ T cells was higher in irradiated Piezo2-/--RE tumors compared with that in Piezo2-deficient tumors (Fig. S2 R).

These data collectively indicated that increased production of cytotoxic cytokines and higher stem cell-like CD8⁺ T cell populations both likely contributed to enhancing the antitumor effects of Piezo2 after KO following ionizing radiation (IR) treatment.

Tumor cell-derived IL-15 is required for improved CD8* T cell-mediated antitumor immunity in irradiated Piezo2 KO tumors

Several types of cytokines are known to play an essential role in T cell differentiation in the TME (Raeber et al., 2018; Propper and Balkwill, 2022). To investigate whether the enhanced antitumor immune response associated with Piezo2 deficiency was related to cytokine production, we performed RNA-seq using Piezo2 KO and WT MC38 tumor cells with or without radiation treatment. Analysis of DEGs indicated that several cytokines commonly released by tumor cells, such as Ilia, Ilib, Il2, Il4, Il5, Il6, Il7, Il11, Il12b, Il13, Il15, Il17a, Il17c, Il17d, Il17f, Il18, Il20, and Il21, tumor cell-derived Il-15 expression showed the greatest increase in irradiated Piezo2 KO cells compared with that in WT tumor cells receiving IR treatment (Fig. 3 A). IL-15 is well-known to stimulate proliferation in CD8+ T cells, which benefits tumor control (Raeber et al., 2018). Further evaluation of Il-15 mRNA expression by Q-PCR in cultured MC38 or B16F1 cells treated with or without radiation confirmed that Il-15 mRNA expression was strikingly higher after radiation in Piezo2-/- cells compared with that in WT cells (Fig. 3 B).

To further investigate the effects of Piezo2 on IL-15 production in vivo, we assessed IL-15 expression in different cell types from irradiated or non-irradiated tumors. The data showed that



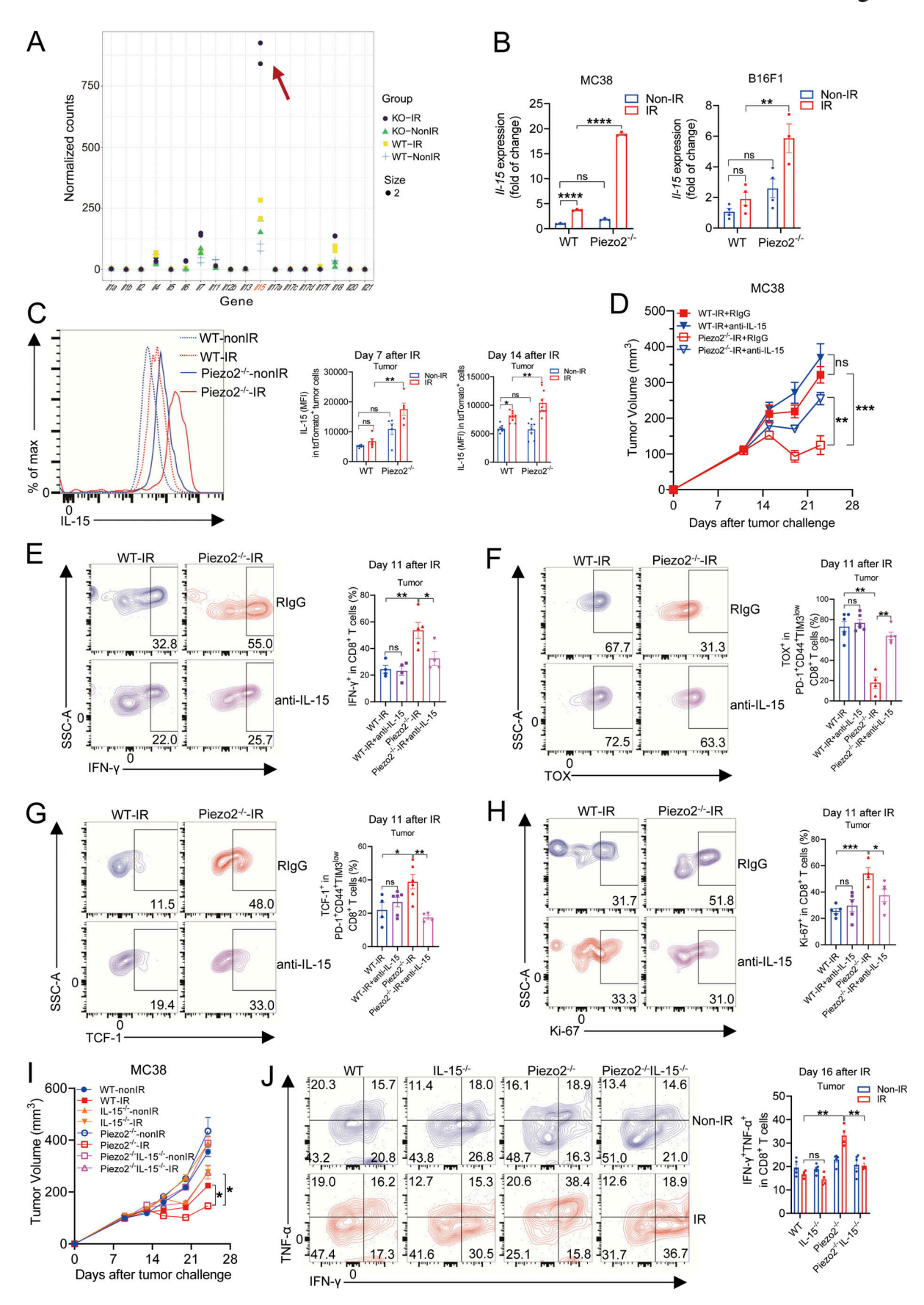


Figure 3. Increase of tumor cell-derived IL-15 is responsible for the enhanced antitumor immunity after radiation by Piezo2 deficiency. (A and B) WT and Piezo2^{-/-} MC38 cells were irradiated at a single fraction of 30 Gy. At 60 h after radiation, total RNA was extracted and further analyzed. (A) RNA-seq



analysis of indicated cytokine mRNA expression. Bar plots from RNA-seq reveal the genes coding T cell-related cytokines. (B) Il-15 mRNA expression in WT and Piezo2^{-/-} MC38 or WT and Piezo2^{-/-} B16F1 with or without radiation was shown from two independent experiments. (C) C57BL/6 were transplanted subcutaneously with 2 × 106 WT MC38-tdTomato and Piezo2^{-/-} MC38-tdTomato cells. Tumors were treated locally with one fraction of 18-Gy IR. On days 7 and 14 after radiation, IL-15 expression in MC38-tdTomato⁺ cells was represented from three independent experiments (n = 5-9 mice per group). (D) C57BL/6 were transplanted subcutaneously with 2 × 10⁶ WT MC38 and Piezo2^{-/-} MC38 cells. Tumors were treated locally with one fraction of 18-Gy IR. Anti-IL-15 was administered intratumor at 100 µg per mouse to mice every 2 days for a total of four times from the day receiving radiotherapy. Tumor growth was measured twice a week. The tumor growth curve was represented from two independent experiments (n = 6 mice per group). (E) Representative data and quantification of the percentage of IFN-y⁺ in CD8⁺ T cells from irradiated WT and Piezo2^{-/-} MC38 tumors with or without anti-IL-15 treatment on day 11 after IR were shown from two independent experiments (n = 4-5 mice per group). (F and G) Representative data and quantification of the percentage of TOX+ (F) and TCF-1+ (G) in $PD-1+CD4+TIM3^{low}CD8+T cells from tumors with or without anti-IL-15 treatment on day 11 after IR were shown from two independent experiments (n = 4-6) and the state of th$ mice per group). (H) Representative data and quantification of the percentage of Ki-67* in CD8* T cells from irradiated WT and Piezo2^{-/-} MC38 tumors with or without anti-IL-15 treatment on day 11 after IR were shown from two independent experiments (n = 4-5 mice per group). (1) C57BL/6 were transplanted subcutaneously with 2 × 10⁶ WT, IL-15^{-/-}, Piezo2^{-/-}, and Piezo2^{-/-}IL-15^{-/-} MC38 cells. Tumors were treated locally with one fraction of 18-Gy IR. The tumor growth curve was represented from two independent experiments (n = 4-6 mice per group). (1) Representative data and quantification of the frequency of IFNγ*TNF-α*CD8+ T cells from irradiated WT, IL-15-/-, Piezo2-/-, and Piezo2-/-IL-15-/- MC38 tumors on day 16 after IR were shown from two independent experiments (n = 4-6 mice per group). Data were represented as means ± SEM. B, C, E-H, and I were calculated by one-way ANOVA with multiple comparison tests. D and I were analyzed by two-way ANOVA with multiple comparison tests. *P < 0.05; **P < 0.01; ***P < 0.001; ****P < 0.001; ****P < 0.0001; ns, no significant difference.

IL-15 was expressed in both CD45⁺ and CD45⁻ cells, with obviously higher IL-15 levels in irradiated tumors (Fig. S3 A). These results suggested that after radiation, IL-15 release from CD45⁻ cells could potentially play a role in enhancing the response to radiation in Piezo2 KO MC38 tumors. Moreover, we analyzed the IL-15 expression in CD4⁺ T cells, CD8⁺ T cells, neutrophils, monocytes, macrophages, and dendritic cells (DCs). The data showed that IL-15 levels in indicated immune cells were similar in WT and Piezo2 KO tumors with or without radiation treatment (Fig. S3 B). On the basis of these results above, we next focused on the effects of Piezo2 deficiency on tumor cell-derived IL-15 expression following radiation.

To further confirm that the increase of IL-15 was induced by irradiated Piezo2^{-/-} tumor cells, we generated an MC38 cell line stably expressing tdTomato to label KO and WT tumor cells in mice. We then isolated tdTomato-labeled cells from tumors and quantified IL-15 using flow cytometry. The flow cytometric analysis indicated that IL-15 expression was higher in tdTomato-expressing cells obtained from Piezo2^{-/-} tumors compared with that in WT tumors on days 7 and 14 following radiation treatment (Fig. 3 C).

In addition, we also assessed whether tumor cell-derived IL-15 was essential for the enhanced antitumor effects of Piezo2 KO in irradiated tumors by blocking IL-15 through intratumoral injection of neutralizing antibodies in vivo. We found that blocking IL-15 reversed the suppression of tumor growth associated with Piezo2 KO in radiation-treated mice but had no effect on irradiated WT tumor growth (Fig. 3 D). Furthermore, we determined the effects of IL-15 blockade on the expression of other functional and differentiation markers in tumor-infiltrating CD8+ T cells. The results demonstrated that the percentage of IFN- γ^+ cells detected among CD8+ T cells was higher in irradiated Piezo2 KO tumors but decreased after IL-15 blockade (Fig. 3 E), while the frequency of TOX+ in exhausted CD8+ T cells was higher after anti-IL-15 treatment in irradiated Piezo2-/- tumors compared with that in Piezo2-deficient tumors without IL-15 blockade (Fig. 3 F). Moreover, the elevated proportions of the CD8⁺ T cell stemness markers expressing TCF-1 and Ki-67 could be attenuated by IL-15 blockade in irradiated Piezo2-/- tumors but not in WT tumors with radiation treatment (Fig. 3, G and H).

To further verify that the increased IL-15 by tumor cells was required for the enhanced antitumor response of irradiated Piezo2 KO tumors, we next generated IL-15 $^{-/-}$ and Piezo2 $^{-/-}$ IL-15 $^{-/-}$ cell lines by CRISPR-Cas9 genome editing. The knockdown efficiency of IL-15 was determined by western blot (Fig. S3 C). Consistent with the data shown in the irradiated Piezo2-/- tumors treated with anti-IL-15, the KO of IL-15 in Piezo2 KO cells could rescue the strengthened tumor growth suppression in Piezo2^{-/-} tumor upon radiation treatment (Fig. 3 I). In addition, the frequency of IFN- γ^{+} TNF- α^{+} observed in CD8+ T cells was higher in irradiated Piezo2 KO tumors but decreased in Piezo2-/-IL-15-/- tumors (Fig. 3 J). Moreover, TCF-1⁺ proportion among exhausted CD8⁺ T cells from irradiated Piezo2^{-/-} tumors was increased compared with that in WT tumors after radiation but decreased in Piezo2 KO tumors due to lack of IL-15 (Fig. S3 D). These results suggested that IL-15 increase in tumor cells after radiation was critical for the enhanced tumor suppression in irradiated Piezo2 KO tumors.

IL-15 binds to the transmembrane domain of IL-15Rα and is subsequently presented in trans to IL-2/IL-15Rβγ heterodimer to activate neighboring CD8+ T cells and natural killer (NK) cells (Fiore et al., 2020; Ma et al., 2022). We next determined whether the Piezo2 KO-induced production of IL-15 could affect IL-15Rα+CD8+ T cell expansion in irradiated tumors. Using flow cytometry, we observed that irradiated Piezo2-/- tumors had a greater increase in IL-15Rα⁺CD8⁺ T cells than that in irradiated WT tumors (Fig. S3 E), although the percentage of IL-15Rα+CD8+ T cells from DLNs did not obviously change after radiation (Fig. S3 F). Correlation analysis between IL-15Ra expression on tumor-infiltrating CD8⁺ T cells and IFN-γ, TCF-1, and Ki-67 expression showed that IL-15Ra shared a strong positive relationship with these stemness and differentiation markers (Fig. S3, G-I). These results further supported that tumor cell-derived IL-15 production in irradiated Piezo2 KO cells strongly promotes CD8⁺ T cell differentiation. We also analyzed IL-15Rα expression on CD4+ T cells, CD8+ T cells, neutrophils, monocytes, macrophages, and DCs in tumors, which contribute to the trafficking of IL-15 to the cell surface. The measurement showed that IL-15R α expression was remarkably changed on CD8+ T cells after radiation in Piezo2 KO tumors, whereas other major immune cells



showed no obvious alterations in IL-15R α expression within tumors (Fig. S3 J). Furthermore, staining of p-STAT5 to evaluate the activation of IL-15R α downstream signaling in tumorinfiltrating CD8+ T cells showed that p-STAT5 expression was higher in CD8+ T cells from irradiated Piezo2-/- tumors compared with that in WT tumors upon radiation treatment (Fig. S3 K). These cumulative results thus indicated that the IL-15/IL-15R α axis was critical for the enhanced radiation-induced antitumor immunity accompanying Piezo2 deficiency.

IRF-1 is essential for enhanced IL-15 production in Piezo2deficient tumor cells following radiotherapy

Previous studies have shown that the expression of IL-15, required for NK cell development and virus recognition, is dependent on IFN regulatory factor-1 (IRF-1) transcriptional regulatory function (Liu et al., 2019; Ma et al., 2022). Based on this proposed role of IRF-1, we next sought to determine whether it also participated in Piezo2 KO-associated increase in IL-15 following tumor cell irradiation. Western blot verified that IRF-1 was expressed mainly in the nucleus and that its expression significantly increased in Piezo2 KO MC38 or B16F1 cells by 60 h after radiation compared with that in irradiated WT cells (Fig. 4 A and Fig. S4 A). Subsequent immunofluorescent staining further illustrated that IRF-1 expression could be induced to higher levels by radiation treatment in Piezo2deficient tumor cells than in tumor cells harboring functional Piezo2 (Fig. S4 B). This increased expression of IRF-1 was also observed by flow cytometry in tdTomato+ Piezo2-/- MC38 tumor cells isolated from irradiated tumors (Fig. 4 B). These results suggested that IRF-1 played a role in Piezo2 KO-associated IL-15 upregulation.

To determine whether IRF-1 is required for Piezo2 KOassociated IL-15 release enhancement, we generated an IRF-1 KO stable cell line by shIRF-1 targeting in Piezo2-/- MC38 and Piezo2-/- B16F1 tumor cells. After confirming that IRF-1 was indeed knocked down by western blot (Fig. S4, C and D), we examined IL-15 production following irradiation in Piezo2^{-/-}IRF-1^{-/-} B16F1 or MC38 cells. We found that IRF-1 KO could abolish the Piezo2 KO-associated increase of IL-15 levels after radiation treatment, displaying comparable levels to that of irradiated WT controls (Fig. 4, C and D). In addition, IRF-1 KO also reversed the enhanced IL-15 production by CD45⁻ cells in irradiated Piezo2 KO tumors as well as the therapeutic effects on tumor size in vivo (Fig. 4, E and F). Furthermore, flow cytometry assessment of the effects of IRF-1 KO on intratumoral CD8+ T cell differentiation showed that the percentage of PD-1+CD8+ T cells was higher in irradiated Piezo2^{-/-}IRF-1^{-/-} tumors compared with that in radiation-treated Piezo2^{-/-} tumors (Fig. 4 G), whereas the proportions of TCF-1+ and CD62L+ cells decreased among total tumor-infiltrating CD8+ T cells under IRF-1 deficiency (Fig. 4, H and I). Taken together, these data demonstrated that IRF-1 was required for the Piezo2 KO-associated increase in IL-15 production and augmented antitumor response to radiotherapy.

Piezo2 deficiency enhances IL-15 production in irradiated tumor cells through JAK2/STAT1/IRF-1 signaling

Treatment with JAK inhibitors induces immunosuppression by disrupting IL-15 and IFN- γ cytokine signaling (Frisoli et al., 2020). To improve our understanding of how JAK/STAT signaling might

contribute to enhancing IL-15 production in the absence of Piezo2, we detected phosphor (p)-JAK2 and -STAT1 levels after irradiation in Piezo2 KO and WT MC38 and B16F1 tumor cells. Western blots showed that p-JAK2 and p-STAT1 levels were markedly higher in irradiated Piezo2 KO tumor cells compared with that in WT cells (Fig. 5 A and Fig. S5 A), and a similar trend in p-STAT1 levels was also observed in tdTomato+-labeled cells isolated from radiationtreated Piezo2 KO tumors in vivo (Fig. 5 B). To confirm whether JAK2/STAT1 pathway activation was essential for upregulation of the IRF-1/IL-15 axis in irradiated Piezo2-/- tumor cells, we administered the JAK2 inhibitor, baricitinib, in cultured tumor cells in vitro. We first validated that p-JAK2 and p-STAT1 levels were decreased in irradiated Piezo2 KO cells with baricitinib treatment (Fig. S5 B). Flow cytometry analysis showed that the increased expression of IL-15 and IRF-1 in irradiated Piezo2^{-/-} MC38 (Fig. 5, C and E) or B16F1 (Fig. 5, D and F) tumor cells was reversed by exposure to JAK2 inhibitor. Of note, inhibition of JAK2-STAT1 signaling in irradiated WT tumor cells by baricitinib had no influence on the induction of IRF-1 and IL-15 compared with that in WT tumor cells receiving radiation without inhibitor treatment.

Previous studies have demonstrated that IFN- γ signaling initiated by IFN- γ binding to IFN- γ receptor, which could induce robust STAT1 phosphorylation and blockade of IFN- γ signaling decreased STAT1 activation (Farrar and Schreiber, 1993; McGillicuddy et al., 2009; Richard and Stephens, 2011; Ivashkiv, 2018; Lang et al., 2019). In view of this, we determined the expression of IFN- γ in tdTomato⁺ cells from tumors and tested the IL-15 expression with or without anti-IFN- γ blockade following radiation. We observed that IFN- γ expression was increased in tdTomato⁺ cells from irradiated Piezo2^{-/-} tumors compared with that in the WT tumor upon radiation treatment (Fig. 5 G). In addition, we found that treatment with anti-IFN- γ after radiation resulted in the decline of IL-15 expression in Piezo2^{-/-} cells, in contrast to that in irradiated cells with Piezo2 deficiency in the absence of anti-IFN- γ (Fig. 5 H).

These observations together indicated that the Piezo2 KO-associated increase in IL-15 expression after radiation was dependent on IFN- γ -triggered JAK2/STAT1 signaling.

Piezo2 expression is related to CD8⁺ T cell infiltration and clinical response to radiotherapy

In light of these results in mice and tumor cell lines, we next explored whether Piezo2 and CD8 expression were correlated with radiosensitivity in clinical samples by immunohistochemistry (IHC) staining.

First, patients with rectum adenocarcinoma (the most common colorectal cancer) after radiotherapy were stratified according to treatment response (i.e., "responder" and "non-responder"). The quantification of IHC showed that responders had significantly decreased Piezo2 expression and increased CD8+ T cell infiltration compared with non-responders (Fig. 6, A and B), suggesting that interrupting Piezo2 signaling could serve as a strategy to overcome treatment resistance. Furthermore, we analyzed the correlation between Piezo2 expression and CD8+ T cell infiltration, and the results indicated that Piezo2 expression in tumor tissue inversely correlated with the infiltration of CD8+ T cells (Fig. 6 C).



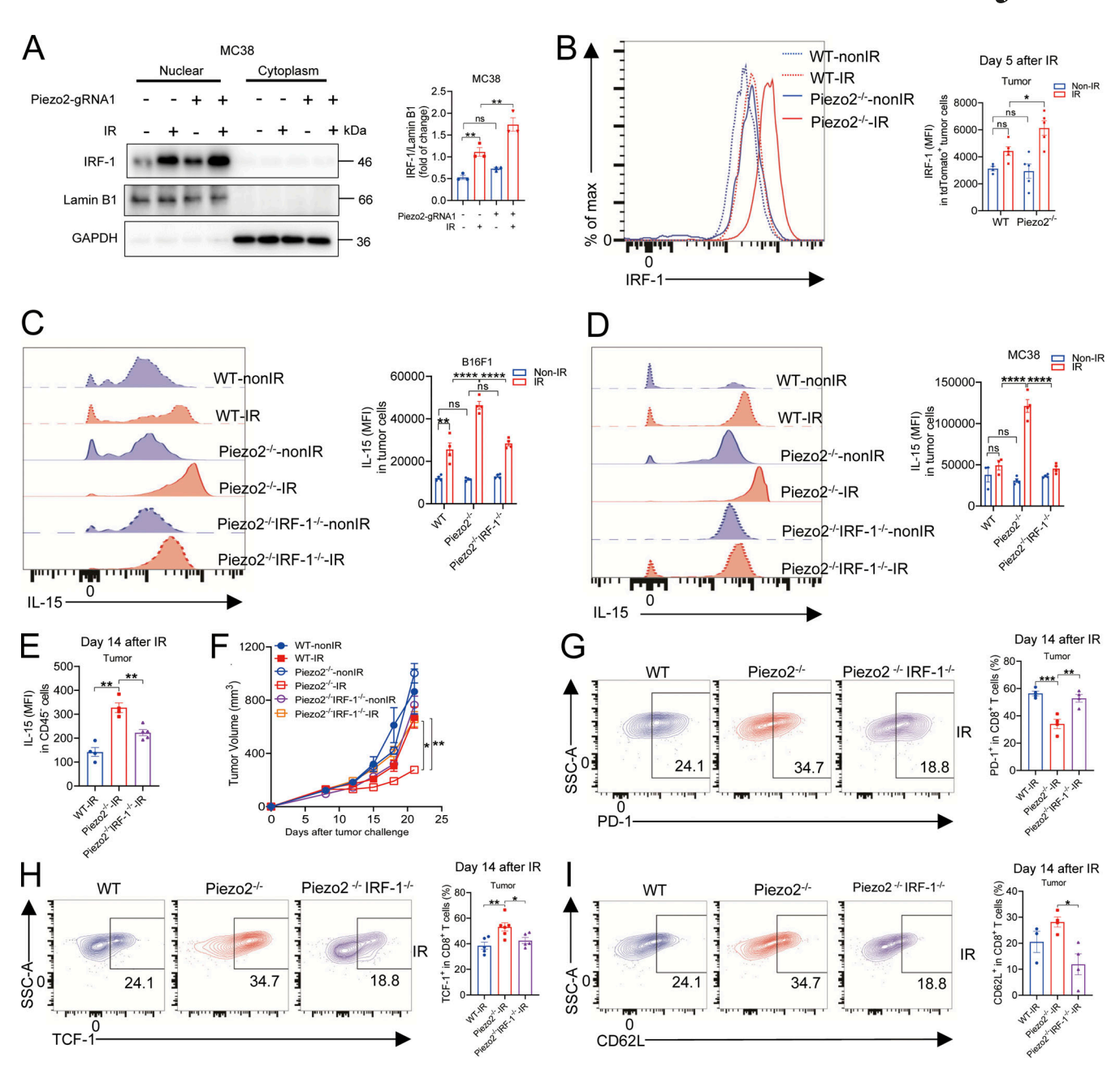


Figure 4. IRF-1 is essential for IL-15 production after radiation in Piezo2 KO tumors. (A) The expression of IRF-1 from nuclear and cytoplasm of WT and Piezo $2^{-/-}$ MC38 by 60 h after IR treatment was shown from three independent experiments. (B) C57BL/6 were transplanted subcutaneously with 2 × 10⁶ WT and Piezo2^{-/-} MC38-tdTomato cells. Tumors were treated locally with one fraction of 18-Gy IR. On day 5 after radiation, IRF-1 expression in MC38-tdTomato cells was analyzed by flow cytometry. Representative data of IRF-1 expression (left) and quantification analysis (right) in irradiated WT and Piezo2^{-/-} MC38 tumors were shown from two independent experiments (n = 3-5 mice per group). (c) At 60 h after IR, IL-15 expression in WT, Piezo2-/-, and Piezo2-/-IRF-1-/-B16F1 tumor cells was shown from three independent experiments. (D) The IL-15 expression in WT, Piezo2^{-/-}, and Piezo2^{-/-}IRF-1^{-/-} MC38 tumor cells by 60 h upon radiation treatment was shown from three independent experiments. (E) The IL-15 expression in CD45⁻ cells from irradiated WT, Piezo2^{-/-}, and Piezo $2^{-/-}$ IRF- $1^{-/-}$ MC38 tumors on day 14 after IR was represented from two independent experiments (n = 4-5 mice per group). (F) C57BL/6 were transplanted subcutaneously with 2×10^6 WT, Piezo2^{-/-}, and Piezo2^{-/-}IRF-1^{-/-} B16F1 cells. Tumors were treated locally with one fraction of 18-Gy IR. The tumor growth curve was shown from two independent experiments (n = 4-6 mice per group). (G) Representative data and quantification of the percentage of PD-1* in CD8+ T cells from irradiated WT or Piezo2-/- MC38 tumors with or without IRF-1 on day 14 after IR were shown from two independent experiments (n = 4 mice per group). (H) Representative data and quantification of the percentage of TCF-1+ in CD8+ T cells from irradiated WT or Piezo2-/- MC38 tumors with or without IRF-1 on day 14 after IR were shown from two independent experiments (n = 5-6 mice per group). (1) Representative data and quantification of the percentage of CD62L⁺ in CD8⁺ T cells from irradiated WT or Piezo2^{-/-} MC38 tumors with or without IRF-1 were shown from two independent experiments (n = 1) 3-4 mice per group). Data were represented as means ± SEM. Statistical analysis was performed by one-way ANOVA with multiple comparison tests (A-E and G-I), and statistical analysis was calculated by two-way ANOVA with multiple comparison tests (F). *P < 0.05; **P < 0.01; ***P < 0.001; ****P < 0.0001; ****P significant difference. Source data are available for this figure: SourceData F4.



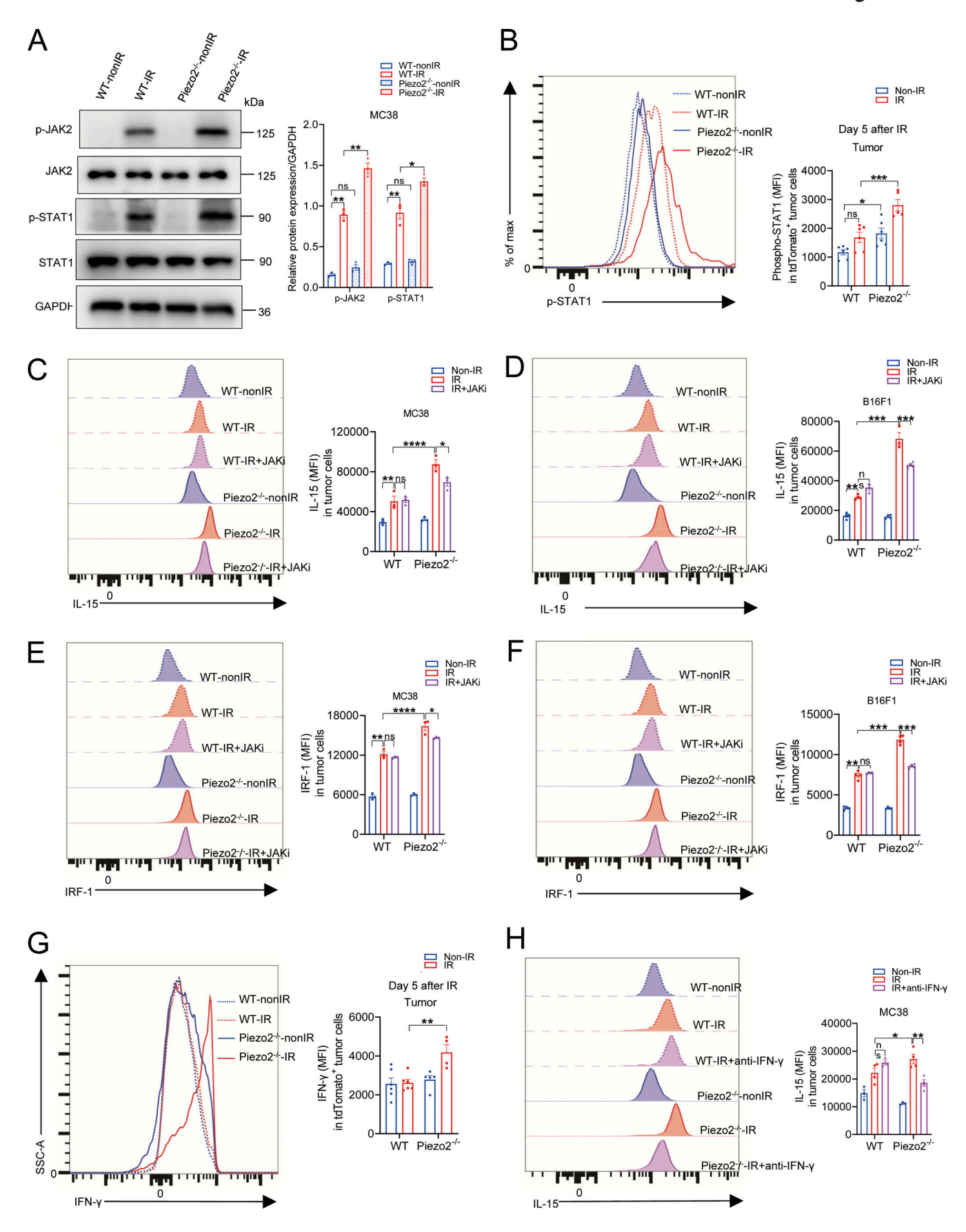


Figure 5. Increase of IRF-1 and IL-15 expression in Piezo2 KO tumor cells upon radiation depended on JAK2/STAT1 pathway. (A) The expression of p-JAK2 and p-STAT1 shown by western blot (left) and quantification (right) in WT and Piezo2^{-/-} MC38 with or without IR treatment for 15 min after IR were



represented from three independent experiments. **(B)** C57BL/6 were transplanted subcutaneously with 2×10^6 WT and Piezo2^{-/-} MC38-tdTomato⁺ cells. Tumors were treated locally with one fraction of 18-Gy IR. On day 5 after radiation, p-STAT1 expression in MC38-tdTomato⁺ cells was analyzed by flow cytometry. Representative data and quantification of p-STAT1 expression in MC38-tdTomato⁺ cells from irradiated tumors were shown from two independent experiments (n = 5-6 mice per group). **(C and D)** Representative data and quantification of IL-15 expression in WT and Piezo2^{-/-} MC38 (C) and B16F1 (D) cells at 15 min after radiation with or without JAK inhibitor ($1 \mu M$) 1 h ahead of IR were shown from three independent experiments. **(E and F)** Representative data and quantification of IRF-1 expression in WT and Piezo2^{-/-} MC38 (E) and B16F1 (F) cells at 15 min after radiation with or without JAK inhibitor ($1 \mu M$) 1 h ahead of IR were shown from three independent experiments. **(G)** Representative data and quantification of IFN- γ expression in WT and Piezo2^{-/-} MC38-tdTomato⁺ cells from tumors on day 5 upon radiation were shown from two independent experiments (n = 4-6 mice per groups). **(H)** Representative data and quantification of IL-15 expression in irradiated MC38 cells with or without anti-IFN- γ treatment at 100 μ g/ml for 60 h are shown from two independent experiments. Data were represented as means ± SEM. Statistical analysis was performed by one-way ANOVA with multiple comparison tests (A–H). *P < 0.05; **P < 0.01; ***P < 0.001; ***P < 0.001;

In addition, we reanalyzed RNA-seq data of pancreatic ductal adenocarcinoma (PDAC) tumor tissue samples from patients following radiotherapy in the Gene Expression Omnibus (GEO) database (GSE225767) (Piper et al., 2023). We found that although there were no statistically significant differences between responder and non-responder, the trend that lower expression of Piezo2 but higher IL-15 expression was associated with better response to radiotherapy was observed in patients with PDAC (Fig. 6, D and E).

Collectively, these analyses of clinical data suggested that Piezo2 might affect the response to radiation treatment in humans and may become a potential target for overcoming radioresistance.

Discussion

In this study, we found that tumor cell size increased after radiation treatment, which was associated with upregulation of the mechanosensitive ion channel, Piezo2, in RNA-seq data. Experimental characterization of Piezo2 function by genetic KO in tumor cells revealed its role in tumor response to radiotherapy via suppression of IRF-1/IL-15 signaling. More specifically, Piezo2 deficiency resulted in enhanced expression of IRF-1 and consequently, IL-15 production, which in turn activated IL-15Ra in CD8+T cells, thus promoting an immune response to radiation treatment in vitro and in vivo. Moreover, we found that JAK2/STAT1 signaling was required for the upregulation of IRF-1 and IL-15 in irradiated Piezo2 KO tumor cells, and Piezo2 expression was also correlated with radiosensitivity in rectal cancer patients receiving radiotherapy.

As a sensory transduction channel mediating the first step in a bioelectrical cascade that translates mechanical inputs into cellular responses, Piezo2 was highly upregulated during radiation by Q-PCR and western blots. These results suggest that Piezo2 might specifically participate in tumor response to radiation, supported by the lack of difference in MC38 or B16F1 tumor growth between WT and Piezo2-/- tumors without radiation, but obvious tumor suppression following radiation in Piezo2 KO tumors. Further experiments are required to determine the mechanism of how radiation stimuli regulate Piezo2 expression.

For the detailed mechanism of how tumor cell-extrinsic or -intrinsic factors affect antitumor response by radiotherapy, some extrinsic factors have been identified with the role in influencing radiation-mediated antitumor immunity. A previous

study has shown that the cross-priming capacity of DCs, induced by radiotherapy, requires cytosolic DNA sensing and subsequently promotes tumor-specific effector CD8⁺ T cell function (Deng et al., 2014). Another study reported that low-dose irradiation programs macrophage differentiation to an iNOS⁺/M1 phenotype that orchestrates T cell function (Klug et al., 2013). For tumor cell-intrinsic factors, several investigations have revealed that caspase 9 signaling and ZBP1-MLKL signaling-induced type I IFN responses, both involved in the process of radiation-mediated antitumor immunity (Han et al., 2020; Yang et al., 2021).

In our study, we found that the mechanical force sensor, Piezo2, acts as an endogenous factor in tumor cells to impede CD8+ T cell-mediated antitumor immune responses by suppressing IL-15 production after radiation. Notably, previous studies have reported that IL-15 is mainly produced by activated myeloid cells, such as monocytes, macrophages, and DCs, and that this signal is critical for NK cell development and memory CD8+ T cell homeostasis (Waldmann and Tagaya, 1999; Xue et al., 2021).

Herein, we observed that IL-15 production was remarkably induced after radiation treatment in cells lacking Piezo2, both in vitro and in vivo. Previous work has shown that radiotherapy resulted in a loss of tolerant status in lymphopenic recipient mice due to CD8+ T cells acquiring effector functions and rejecting tumors in an IL-15-dependent fashion (Oelert et al., 2010), which was consistent with findings in our current study. These results suggest that IL-15 combined with radiotherapy might suppress tumors more effectively than either treatment alone. Another interesting study demonstrated that redirecting IL-15 to intratumoral CD8+ T effector cells contributes to better tumor control (Shen et al., 2022). However, although IL-15 appears to be an attractive candidate treatment for cancer, its therapeutic application remains problematic and should be considered with caution (Ma et al., 2022). Therefore, a comprehensive, mechanistic understanding of IL-15 upregulation in irradiated tumor cells could uncover a safer means of triggering IL-15 production to activate tumor immune response. It is possible that suppressing tumor cell-intrinsic Piezo2, as reported here, could potentially enhance IL-15 release after radiotherapy, subsequently augmenting CD8+ T cell function in human cancer patients.

We also examined how IL-15 was upregulated after radiation in the absence of Piezo2 and found that IL-15 upregulation in response to radiation required IRF-1 in tumor cells, which aligned well with previous reports of IL-15 transcriptional regulation.



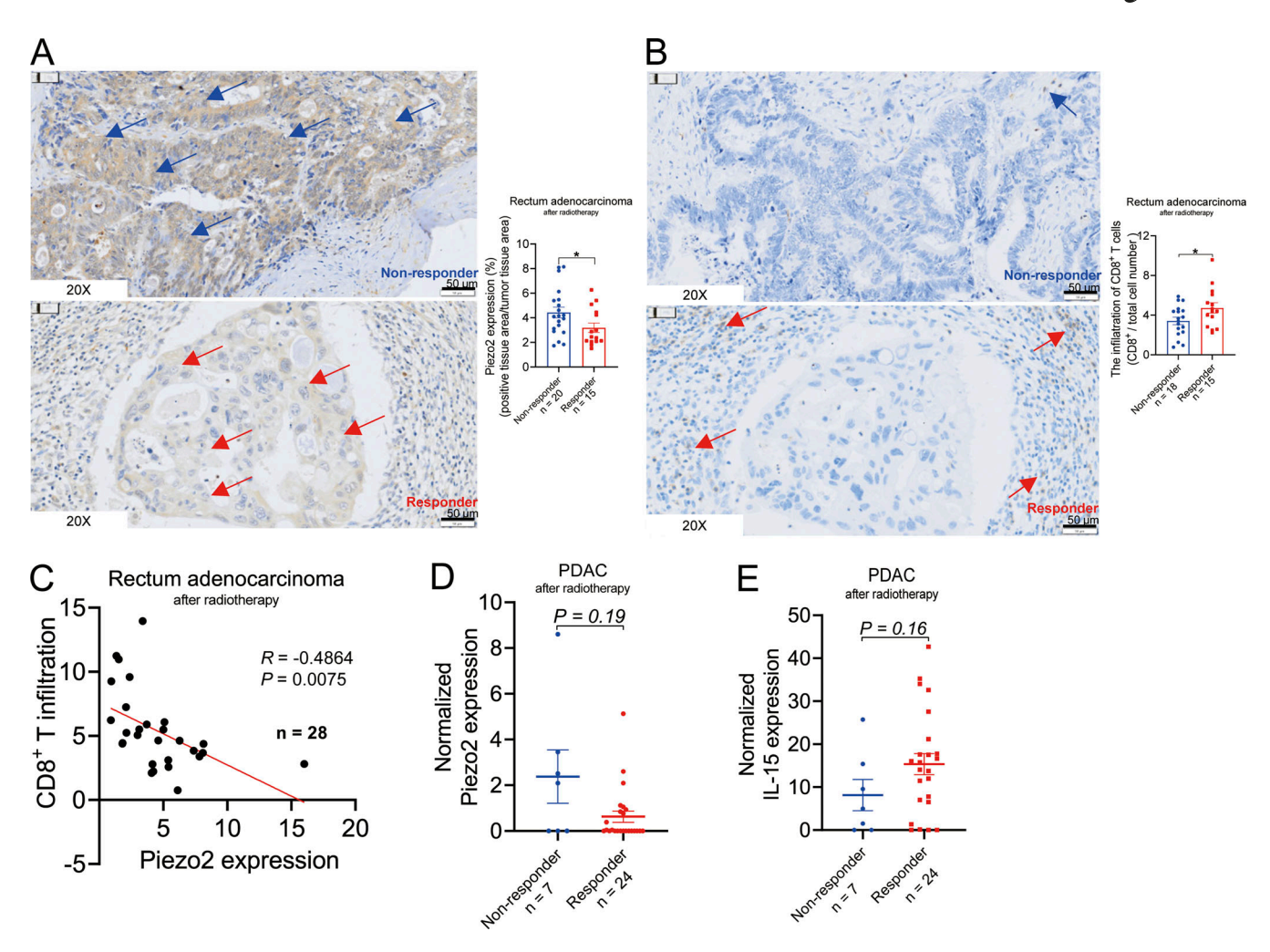


Figure 6. Correlation analysis between Piezo2 expression and radiosensitivity in the clinic. (A) The expression of Piezo2 in tumor samples from patients with rectum adenocarcinoma (READ) post-radiotherapy stratified by responders (n = 15) and non-responders (n = 20). Scale bar = 50 μ m. The blue and red arrows show the expression of Piezo2 detected by immunohistochemistry in non-responder and responder, respectively. (B) The infiltration of CD8+ T cells in tumor samples from patients with READ after radiotherapy grouped by responders (n = 15) and non-responders (n = 18). Scale bar = 50 μ m. The blue and red arrows show the expression of CD8 detected by immunohistochemistry in non-responder and responder, respectively. (C) The correlation between Piezo2 expression and CD8+ T cell infiltration in READ tumor tissue samples following radiotherapy (n = 28). (D and E) Normalized Piezo2 (D) and IL-15 (E) expression in PDAC tumor tissue samples collected after radiotherapy stratified by responders (n = 24) and non-responders (n = 7) in the public database. Data were represented as means \pm SEM. Statistical analysis was performed by unpaired Student's t test (A, B, and E). The correlation between Piezo2 and CD8 infiltration was analyzed by Linear regression of Correlation built in GraphPad Prism 8.0 (C). The comparisons of two nonparametric datasets were calculated by the Mann–Whitney U test (D). *P < 0.05.

One seminal study reported that IRF-1 $^{-/-}$ bone marrow cells treated with exogenous IL-15 can generate functional NK cells and that IL-15 is transcriptionally regulated by IRF-1 (Ogasawara et al., 1998). Another more recent report showed that the cytosolic viral RNA-sensing receptor RIG-I in APCs can maintain intestinal intraepithelial lymphocytes via a MAVS-IRF-1-IL-15 axis-dependent manner (Liu et al., 2019), thus supporting the positive regulation of IL-15 by IRF-1. In addition, IRF-1 was shown to play a critical role in response to liver injury via regulation of IL-15/IL-15R α (Yokota et al., 2015).

The JAK2/STAT1 pathway was previously identified as a major regulator of IRF-1 expression (Horiuchi et al., 2000). Our data also showed that p-JAK2 and p-STAT1 levels were higher in irradiated Piezo2 KO cells, along with upregulation of IRF-1, compared with that in cells expressing WT Piezo2. This positive

regulatory role of JAK2/STAT1 was further supported by the loss of radiation-induced IRF-1/IL-15 expression by treatment with the JAK2 inhibitor.

It is noticeable that IL-15 and IRF-1 expression in WT tumor cells was remarkably increased after radiation treatment, but there was no impact on their induction in the presence of the JAK inhibitor. Unlike the observation in the WT tumor cell, the enhanced induction of IL-15 and IRF-1 in irradiated Piezo2-/-cells could be abrogated after the treatment of JAK inhibitor. These data demonstrated that the IRF-1/IL-15 expression was partially mediated by JAK2-STAT1 signaling in WT tumor cells upon radiation treatment, but in contrast to irradiated WT cells, the increased expression of IRF-1 and IL-15 in irradiated Piezo2-/- cells was completely dependent on the JAK2-STAT1 pathway. We next sought to find whether the IFN- γ



signaling, an upstream process to initiate JAK2-STAT1 cascade (Ivashkiv, 2018), was involved in Piezo2 KO-associated IL-15 upregulation. We discovered that treatment with anti-IFN- γ abolished the effect of Piezo2 deficiency on IL-15 increase following radiation treatment. However, further study is needed to determine the mechanism by which Piezo2 modulates IFN- γ production.

In summary, our study defines a new tumor cell-intrinsic factor, Piezo2, as a suppressor of radiation-induced antitumor immune responses by inhibition of their IL-15 production. By contrast, Piezo2 ablation in tumor cells promotes their production of IL-15 via p-JAK2/p-STAT1/IRF-1 activation to trigger stem cell-like features of tumor-infiltrating CD8⁺ T cell and enhance their effector function after radiation treatment.

In the end, our observations in mouse models were further validated by the clinical results demonstrating that Piezo2 expression was inversely correlated with radiosensitivity. In the future, we believe studies in additional cancer types prior to or post radiotherapy are warranted to assess whether Piezo2 could be a useful biomarker for predicting radiotherapy efficacy. Based on our results, we also propose that targeting the Piezo2 pathway in combination with radiotherapy could provide a potentially effective strategy to further improve radiation-induced antitumor immunity and increase tumor sensitivity to radiotherapy.

Materials and methods

Study design

This study was designed to determine whether the mechanical force sensor Piezo2 contributes to antitumor effects in MC38 and B16F1 tumors with radiation treatment, to assess whether Piezo2 affects CD8+ T cell-mediated antitumor immune response induced by radiotherapy, and to characterize the role of Piezo2 on IL-15 production. Tumor size and stretch of cell skeleton were evaluated using scanning electron microscopy, flow cytometry, and immunofluorescence staining in mouse tumor cells. To investigate the direct role of Piezo2, IL-15, and IRF-1 in tumor cells, Piezo2-/-, IL-15-/-, IRF-1-/-, and Piezo2-/-IL-15-/-, Piezo2^{-/-}IRF-1^{-/-} cell lines were generated using CRISPR-Cas9 technology and shRNA. We monitored tumor growth and analyzed the infiltration, function, and differentiation of CD8+ T cells in the tumor and DLNs. To further determine the effects of tumor cell-derived IL-15 on CD8+ T cells, IL-15-neutralizing antibody injection and IL-15 knockdown in Piezo2 KO cells were applied in tumor treatment. Last, to determine how Piezo2 affects tumor cell-intrinsic IL-15 expression, the activation of the JAK2/STAT1/IRF-1 pathway was detected by western blot and flow cytometry. Furthermore, we also performed IHC staining on clinical samples and reanalyzed bulk RNA-seq data from a public database to confirm whether Piezo2 was involved in the antitumor response in human cancer with radiation treatment.

In our study, for cell-based experiments, at least biological triplicates were performed in each single experiment, unless otherwise stated. Animals were randomized into different groups after tumor cell inoculation and at least three to nine mice were used for each group, unless otherwise indicated. Animals that failed to develop tumors from the beginning were

excluded from the analysis. Analytical studies were typically performed two to three times in independent experiments, implementing fixed time points of analysis for all experimental groups, unless indicated.

Mice

6- to 8-wk-old female C57BL/6 (WT) mice were purchased from Shanghai Slac Laboratory Animal Co. Ltd. OT-I transgenic mice (CD45.1*) were kind gifts from Dr. Q. Zou (Shanghai Institute of Immunology, Shanghai, China). All the mice were maintained under specific pathogen-free conditions at the animal facility of Shanghai Jiao Tong University School of Medicine. All the animal studies were conducted in compliance with the protocol approved by the Institution Animal Care and Use Committee of Shanghai Jiao Tong University School of Medicine (no. A-2022-019).

Cell lines and culture conditions

MC38, MC38-OVA, and B16F1 were contributed by the laboratory of L.-F. Deng (Shanghai Jiao Tong University, Shanghai, China); 293T and Phoenix were gifts from F.-B. Li (Shanghai Institute of Immunology, Shanghai, China). These cell lines were cultured at 37°C with 5% CO2 in Dulbecco's modified Eagle's medium-high glucose medium (Corning) containing 10% fetal bovine medium (FBS) (ExCell Bio.), penicillin (100 U/ml), streptomycin (100 µg/ml), and 10 mM Hepes (Thermo Fisher Scientific). All cell lines were tested to be mycoplasma-free. Piezo2^{-/-} MC38, Piezo2^{-/-} MC38-OVA, Piezo2^{-/-} B16F1, IL-15^{-/-}, and Piezo2^{-/-}IL-15^{-/-} MC38 were generated using CRISPR-Cas9 plasmid lenti-crispr-V2 (from the laboratory of L.-F. Deng). The annealed single-guide RNA oligos (see Table S1) were cloned into pLenti-CRISPR-V2 and packaged in 293T cells. Supernatants containing virus particles were collected 24 and 48 h after transfection and then added to preplated cells with polybrene (2 µg/ml, Genomeditech). The transduced cells were selected by puromycin (Beyotime Biotechnology) at 2 µg/ml to acquire the gene-deleted stable cell lines. The efficiency of gene knockdown was determined by western blot. Also of note, we applied two pairs of gRNAs mix to silence IL-15 expression and generated polyclonal IL-15^{-/-} and Piezo2^{-/-}IL-15^{-/-} MC38 cell lines. In addition, tdTomato-expressing WT MC38 and tdTomato-expressing Piezo2^{-/-} MC38 were generated using pLenti-CMV-tdTomato (from the laboratory of L.-F. Deng). For the generation of the Piezo2-RE cell line, we acquired the plasmids (81073-mPiezo2-CMV-Sport6 and 25426-pCMVSport6/mPax3) from ADDGENE. We transfected B16F1 with these two plasmids separately by Lipofectamine 3000 Reagent (Thermo Fisher Scientific) followed by the monoclonal screening. For the generation of Piezo2^{-/-}IRF-1^{-/-} MC38 and B16F1 cell lines, we applied Phoenix to package retrovirus. First, Phoenix cells preplated in 100-mm dishes were transfected with pSIREN-RetroQ-ShRNA-scramble or pSIREN-RetroQ-ShRNA-irf-1 (see Table S1) using 10 µl Neofect DNA transfection reagents (MayinTech). On days 2 and 3, retroviral supernatants were harvested and filtered. Piezo2-/- MC38 cells cultured in 6-well plates were infected with 1 ml supernatants mixed with 1 ml complete medium in the presence of polybrene for the first time. 24 h later, cells were reinfected with the



retroviral supernatants again as described above. The transfection and knockdown were confirmed by western blot.

In vivo tumor models and treatments

To investigate the effects of radiation on tumor growth, WT mice were subcutaneously inoculated with 2 × 106 WT and Piezo2-/-MC38 or WT and Piezo2^{-/-} B16F1 cells, which were resuspended in the phosphate-buffered saline (PBS, 100 µl). Tumors were measured, randomly grouped, and locally irradiated at a single fraction of 18 Gy on the indicated day, and then tumors were monitored twice a week afterward. Briefly, the established tumors (80-150 mm³ in size) were locally irradiated using RS-2000 Biological Irradiator (Rad Source Technologies), while the rest of the mouse body was protected from radiation by a lead shield. For the detection of abscopal effects of radiation, WT mice were inoculated with 2 \times 10 6 WT MC38 or Piezo2 $^{-/-}$ MC38 cells resuspended in PBS on the right flank and with 1×106 WT MC38 cells resuspended in 100 µl PBS on the corresponding opposite flank of the same mice. Tumors on the right flank were subjected to local radiation at a single fraction of 18 Gy, while tumors on the left flank were shielded from radiation. Subsequently, tumors on both flanks were monitored twice a week. To deplete CD8+ T cells, mice were intraperitoneally treated with anti-CD8 antibody at 200 μg/ mouse (A2102, clone 2.43; Selleck, RRID: AB_3099521) every 2 days for three times. For the IL-15 blockade experiments, anti-IL-15 (BE0315, clone AIO.3; Bio X Cell, RRID: AB_2754553) was administered intratumor at 100 µg per mouse to mice every 2 days for a total of four times. For the anti-IFN- γ blockade experiments, cells were treated with anti-IFN-y (BE0055, XMG1.2; Bio X Cell, RRID: AB_1107694) at 100 µg/ml for 60 h.

For the adoptive transfer of OT-I CD8 $^+$ T cell transfer, cells obtained from lymph nodes of OT-I transgenic mice were stimulated with 250 ng/ml OVA peptide (S7951; Sigma-Aldrich) for 24 h in the U-bottom 96-well plates. After 24 h, cells were harvested and replated in 24-well plates with mIL-7 (10 ng/ml; 217-17; Peprotech) and mIL-15 (10 ng/ml; 210-15; Peprotech) for another 3 days. MC38-OVA tumor-bearing mice were irradiated with a dosage of 18-Gy. The next day, OT-I CD8 $^+$ T cells (2 × 10 6 cells/mouse) were intravenously transferred into mice. On day 11 after radiation, further analysis of flow cytometry was performed.

Immunofluorescence

Cells were seeded onto poly-d-lysine-coated confocal dishes at a density of 3×10^4 in 150 μ l complete medium. Cells were irradiated at a single fraction of 30 Gy. After 60 h, cells were stained with Phallodin (40736ES75; Yeason) for 15 min at 37°C. Then the cells were fixed by 4% paraformaldehyde in PBS for 15 min at 37°C. After washing with PBS twice, cells were added with 0.05% Triton-X for 15 min at 4°C. Then the cells were blocked with 3% bovine serum albumin (BSA) and 3% normal goat serum in PBS for 60 min at 4°C. For the cell skeleton staining, the cells were then incubated with anti-pan Cytokeratin antibody (ab7753; Abcam, RRID: AB_306047) overnight at 4°C. After washing with PBS twice, the cells were incubated with a 1:200 dilution secondary antibodies (A0453; Beyotime, RRID: AB_2890132) for 2 h. Hoechst (H1399; Thermo Fisher Scientific) was diluted in 1:500 and stained for 15 min in the dark.

For the IRF-1 staining, the cells were then incubated with anti-IRF-1 antibody (8478; Cell Signaling Technology, RRID: AB_10949108) overnight at 4°C. After washing with PBS for twice, the cells were incubated with a 1:200 dilution secondary antibodies (A0453; Beyotime) for 2 h. Hoechst was diluted in 1:500 and stained for 15 min in the dark. Images were captured with FV3000 confocal system (Olympus), and data were analyzed with Imaris (Bitplane, V9.5) and ImageJ (National Institutes of Health, V2.0.0).

Cell membrane and cytosol protein extraction

Cell membrane and cytoplasmic fractions in tumor cells were extracted using the Membrane and Cytosol Protein Extraction Kit (P0033; Beyotime), according to the manufacturer's instructions. Briefly, sorted tdTomato $^+$ MC38 tumor cells from tumors were collected and lysed in 1 mM PMSF-containing buffer A for 15 min and freeze-thawed three times with liquid nitrogen. The supernatant was collected to remove the nuclei and unbroken cells by spinning at 700 g for 10 min at 4°C. The supernatant was then collected as cytoplasm after spinning at 14,000 g for 30 min at 4°C. The cell membrane fractions were re-suspended in buffer B and incubated on ice for 15 min, followed by vortexing for 5 s at ultrahigh speed three times. Then membrane proteins containing supernatants were collected by centrifugation at 14,000 g for 5 min at 4°C. Proteins were separated on SDS/PAGE and immunoblotted.

Nuclear and cytoplasmic protein extraction

MC38 and B16F1 cells were collected for nuclear and cytoplasmic protein extraction according to the kit (P0028; Beyotime). In detail, the cells were first digested with 0.25% pancreatic enzyme. Adherent cells were scraped and the cell pellet was obtained by centrifugation at room temperature for 5 min 500 µl cytoplasmic protein extraction reagent A containing PMSF (1 mM) was added for 50 µl cell pellet. The cell pellet was completely dispersed by vertexing for 5 s. Then the sample was placed in an ice bath for 15 min 25 µl of cytoplasmic protein extraction reagent B was added to the cell pellet. The mixture was then vortexed at the highest speed for 5 s followed by placing it in an ice bath for 1 min. The sample was centrifuged at 14,000 g at 4°C for 5 min. The supernatant was the cytoplasmic protein fraction. Afterward, 125 µl of nuclear protein extraction reagent containing PMSF (1 mM) was added to the cell pellet. The mixture was subjected to an ice bath and vortexed for 10 s every 2 min for 30 min. Finally, the cell pellet was centrifuged at 14,000 g at 4°C for 5 min. The supernatant was the nuclear protein. The nuclear and cytoplasmic proteins were immediately stored at -80°C.

Western blotting analysis

Samples were acquired from nuclear and cytoplasmic proteins. An equal amount (30 μg per sample) of total protein was loaded and separated by SDS-PAGE and then electrophoretically transblotted onto a polyvinylidene difluoride (PVDF) membrane. The PVDF membrane was blocked in 5% BSA in 1× TBST for 1 h to remove the non-specific binding and then incubated with primary antibodies overnight at 4°C and secondary antibodies at room temperature for 2 h. Finally, the target protein was then imaged with the ImageQuant LAS4000 mini system (GE Healthcare).



The primary antibodies used were anti-Piezo2 (NBP1-78624; NOVUS, RRID: AB_11005294), anti-IL-15 (ab273625; Abcam, RRID: AB_3099515), anti-IRF-1 (8478; Cell Signaling Technology, RRID: AB_10949108), anti-Lamin B1 (12987-1-AP; Proteintech, RRID: AB_2136290), anti-GAPDH (60004-1-lg; Proteintech, RRID: AB_2107436), anti- β -actin (23660-1-AP; Proteintech, RRID: AB_2879307), anti-p-JAK2 (4406; Cell Signaling Technology, RRID: AB_10706164), anti-JAK2 (3230; Cell Signaling Technology, RRID: AB_2128522), anti-p-STAT1(9167; Cell Signaling Technology, RRID: AB_561284), and anti-STAT1 (9172; Cell Signaling Technology, RRID: AB_2198300) antibodies. The secondary antibodies used were HRP-labeled goat anti-rabbit antibodies (A0208; Beyotime, RRID: AB_2892644). The band intensities were quantified using ImageJ software (National Institutes of Health, V2.0.0).

Scanning electron microscope

MC38 cells were seeded on poly-d-lysine-coated coverslips in 6-well plates at a density of $1.5 \times 10^5/\text{ml}$. Cells were irradiated at 30 Gy. After 60 h, cells were fixed with 2.5% glutaraldehyde (dissolved in phosphate buffer) at 4°C for 2 h. After washing with phosphate buffer two times, cells were fixed with 1% osmic acid at 4°C for 2 h. Then the cells were washed with distilled water twice. 30%-50%-70%-80%-95%-100% ethanol was added to the dehydrated sample step by step, 10 min each time. Epoxypropane was added to substitute ethanol. Then the sample was added with Epon812 and epoxypropane at a ratio of 1:1 for 2 h, Epon812 and epoxypropane at a ratio of 2:1 overnight, and subsequently pure epoxypropane 37° C for 6 h. The sample was put in the dryer for 48 h and cut by ultramicrotome (LEICA EM UC7). Lead citrate was added to the sample for electronic staining. The images were taken by scanning electron microscope (FEI QUANTA 200).

Q-PCR

Total RNA for real-time PCR assay was extracted and purified using the TRIzol Reagent (Thermo Fisher Scientific). Reverse transcription reactions were performed with ReverTra Ace qPCR RT Master Mix with gDNA Remover (FSQ-301; Toyobo) following the standard protocol. Quantitative reverse transcription PCR was performed with SYBR Green Realtime PCR Master Mix (QPK-201; Toyobo) in the ViiA 7 Real-Time PCR System with 384-well block (Applied Biosystems). The expression of mRNA was normalized) against glyceraldehyde-3-phosphate dehydrogenase (GAPDH) by the change in cycling threshold (ΔCt) method. Primers used in this study are shown in Table S1.

Flow cytometry

To obtain single-cell suspensions, tumor tissues were cut into small pieces and digested by 1 mg/ml collagenase I (LS004186; Worthington Biochemical) and 0.2 mg/ml DNase I (DN25; Sigma-Aldrich) for 30 min at 37°C. For staining, single-cell suspensions were blocked with anti-FcR (BE0307; Bio X Cell, clone 2.4G2, RRID: AB_2736987) and stained with antibodies against CD45.2 (109839; Biolegend, RRID: AB_2563056), PD-1(135224; Biolegend, RRID: AB_2563523), CD44 (103044; Biolegend, RRID: AB_2561391), TIM3 (119716; Biolegend, RRID: AB_2571932), CD62L (104432; Biolegend, RRID: AB_2285839),

IL-15Rα (153505; Biolegend, RRID: AB_2734220), Ki-67 (652413; Biolegend, RRID: AB_2562664), IFN-γ (505836; Biolegend, RRID: $AB_{2650928}$, $TNF-\alpha$ (506304; Biolegend, RRID: AB_{315425}), Slamf6 (740823; BD, RRID: AB_2740481) and TOX (50-6502-82; eBioscience, RRID: AB_2574265), TCF-1 (566692; BD, RRID: AB_2869822). Dead cells were excluded with Live/Dead Dye (Fixable Viability Stain 700, 564997; BD Bioscience, RRID: AB_2869637). For intracellular staining of transcription factors, TOX, Ki-67, and cytokines, cells were fixed with the Foxp3/ Transcription Factor Staining Buffer Set (eBioscience) in accordance with the manufacturer's instructions. Before intracellular staining of cytokines, cells were stimulated with Cell Stimulation Cocktail (plus protein transport inhibitors) for 4 h. For p-STAT5 and p-STAT1 staining, cells were fixed with PhosflowTM Fix Buffer I (BD) according to BD Phosflow protocol. The first antibody, rabbit anti-mouse p-STAT5 (4322; Cell Signaling Technology, RRID: AB_10544692) or rabbit anti-mouse p-STAT1 antibody (9167; Cell Signaling Technology, RRID: AB_561284), was added at a dilution of 1:200 separately. After the incubation of the first antibody, the second antibody, donkey anti-rabbit IgG Alexa Flour 488 (Poly4064; Biolegend, RRID: AB_2563203), was added at a dilution of 1:2,000. Cells were washed twice with Phosflow Perm/Wash buffer I (BD) and subjected to flow cytometry. Samples were acquired on an LSRII flow cytometer using FACSDiva software (BD Biosciences) and further analyzed with FlowJo software (Tree Star).

For in vivo IL-15 intracellular staining of tumors, cells were fixed with the Foxp3/Transcription Factor Staining Buffer Set (eBioscience) in accordance with the manufacturer's instructions. The first antibody, rabbit anti-mouse anti-IL-15 (ab273625; Abcam, RRID: AB_3099515), was added at a dilution of 1:200. After the incubation of the first antibody, the second antibody, donkey anti-rabbit IgG Alexa Flour 488 (406416; Biolegend, RRID: AB_2563203) was added at a dilution of 1:2,000. It should be noted that for in vivo IL-15 intracellular staining of MC38-tdTomato cells in tumor, due to the influence of fixation buffer on fluorescence quenching of tdTomato, tdTomato needs to be stained first with rat anti-tdTomato antibody (5f8; Chromo Tek, RRID: AB_2336064) followed by the second antibody, goat anti-Rat IgG Alexa Flour 594 (405422; Biolegend, RRID: AB_2563301) before the staining of IL-15 with rabbit anti-IL-15 antibody.

For in vitro IL-15 intracellular staining, to retain IL-15 in the cytoplasm, cells were added to the protein transport inhibitor (555029; BD, RRID: AB_2869014) at a dilution of 1:1,000 ahead of 4 h before we harvested the cells, and cells were fixed with the Foxp3/Transcription Factor Staining Buffer Set (eBioscience) in accordance with the manufacturer's instructions. The first antibody, rabbit anti-mouse anti-IL-15 (ab273625; Abcam, RRID: AB_3099515), was added at a dilution of 1:200. After the incubation of the first antibody, the second antibody, donkey anti-rabbit IgG Alexa Flour 488 (406416; Biolegend, RRID: AB_2563203), was added at a dilution of 1:2,000. Cells were washed twice with Perm/ Wash buffer (eBioscience) and subjected to flow cytometry.

Ca2+ measurement

Cytosolic Ca²⁺ concentration in tumors was measured using Fluo-4 (40704ES50; Yeasen Biotech Co.). In brief, single-cell



suspension from tumors was firstly washed twice with Hank's balanced Salt Solution (HBSS) followed by the treatment with Fluo-4 (final concentration, 5 $\mu M)$ in HBSS at 37°C for 30 min. Then cells were washed twice with HBSS to remove Ca²+ detection probes and cultured with HBSS again at 37°C for another 30 min. Changes in fluorescence intensity were monitored on the BD flow cytometer.

Patients and samples

First, the study protocol of human samples was approved by the central ethics committee of Fudan University Shanghai Cancer Center and the institutional review board (IRB1508151-1) of the Fudan University Shanghai Cancer Center. All participants provided written informed consent.

In brief, tumor samples prospectively collected from patients with rectum adenocarcinoma (the most common colorectal cancer) after radiotherapy were used for the assessment of Piezo2 expression (%-Piezo2 positive tissue area/tumor tissue area) and CD8 infiltration (CD8+ cell number/total cell number) using anti-Human Piezo2 (NBP1-78624; Novus, RRID: AB_11005294) and anti-human CD8 (ab237709; Abcam, RRID: AB_2892677) by IHC. Images of slides were captured using Olympus Slide View VS200, and data were analyzed with HALO Quantitative Image Analysis for Pathology.

For the detailed procedures of treatment for cancer, patients were eligible if they were aged 18–75 years and had histopathologically confirmed rectal adenocarcinoma located $\leq\!10$ cm above the anal verge and clinical stage T3–4 and/or N+ disease on pelvic magnetic resonance images. Patients received pelvic radiation at a dose of 50 Gy/25 fractions via intensity-modulated radiation therapy with concurrent capecitabine 825 mg/m² twice daily for 5 days/wk (neoadjuvant chemoradiotherapy, or nCRT). Total mesorectal excision was scheduled for 8 wk after completion of nCRT.

To group patients based on response to radiotherapy, resected tumors were examined in their entirety, and tumor regression was assessed as identified on routine hematoxylin and eosin staining. We used the American Joint Committee on Cancer (eighth edition) four-tier tumor regression grade (TRG) system to evaluate the response to nCRT and accordingly divided patients into two groups. Among the 35 patients with locally advanced rectal cancer, 15 patients with TRG scores of 0–1 were grouped as responders, and 20 patients with TRG scores of 2–3 were grouped as non-responders.

Statistical analyses

No statistical method was used to predetermine the sample size. Mice were assigned at random to treatment groups for all mouse studies (n=3-9 mice/group). Experiments were repeated two to three times. Statistical analysis was performed using GraphPad Prism8 software (GraphPad Software, Inc.) and presented as stated in individual figure legends. For comparisons between two groups in animal and cell experiments, P values were calculated using Student's t tests. The comparisons of two non-parametric datasets were calculated by the Mann-Whitney U test. For comparisons between three or more groups, P values were calculated using analysis of variance (ANOVA). Data are

presented as mean values \pm SEM. We indicated significance corresponding to the following: *P < 0.05; **P < 0.01; ***P < 0.001; ***P < 0.001; ****P < 0.001; ****P < 0.001; ****P < 0.0001; ***P < 0.0001;

Online supplemental material

Fig. S1 shows cytoskeleton staining, the increase of Piezo2 expression upon radiation in MC38 and B16F1 cells, and the change of Ca²⁺ density in tdTomato⁺ cells from irradiated tumors. Fig. S1 also contains the Piezo2 knockdown efficiency by CRISPR-Cas9 and cell viability determination in WT and Piezo2^{-/-} cells. Fig. S2 contains the frequency of Ki-67+, TCF-1+, CD62L+, or TOX+ in PD-1+CD44+TIM3lowCD8+ T cells, PD-1+, or mean fluorescence intensity (MFI) of Slamf6 in tumor-infiltrating CD8+ T cells. Fig. S2 also includes the percentage of CD8+ in CD45+ cells, IFN-γ+TNF- α^+ , IFN- γ^+ , MFI of Ki-67, and TCF-1+ within CD8+ T cells in DLNs. Piezo2 knockdown efficiency by CRISPR-Cas9 in MC38-OVA cells and Piezo2 expression in Piezo2-/--RE cells is displayed in Fig. S2. Fig. S2 also contains Ca²⁺ density, the percentage of CD8+ in CD45⁺ cells, the frequency of IFN-γ⁺ and TOX⁺ in CD8⁺ T cells in irradiated WT, and Piezo2 $^{-/-}$ and Piezo2 $^{-/-}$ -RE tumors. Fig. S3 shows the analysis of IL-15 expression in indicated populations within tumors and IL-15 knockdown efficiency by CRISPR-Cas9 in MC38 cells. Fig S3 also contains the percentage of TCF-1+ in exhausted CD8⁺ T cells from Piezo2^{-/-}IL-15^{-/-} tumors, IL-15Rα⁺ on CD8+ T cells from tumors, and DLNs. In addition, Fig. S3 shows the correlation of IFN-γ, Ki-67, or TCF-1 with IL-15Rα among different groups separately, MFI of IL-15Rα on indicated subsets of immune cells within tumors, and the expression of phosphor-STAT5 in CD8+T cells from irradiated tumors. Fig. S4 shows IRF-1 expression from nuclear and cytoplasm by western blot and immunofluorescence staining in B16F1 cells, and the knockdown efficiency of IRF-1 using shRNA silencing in Piezo2^{-/-} MC38 and B16F cells. Fig. S5 contains the data of JAK2/STAT1 activation in B16F1 cells and the suppression of phosphor-JAK2/ STAT1 expression by JAK inhibitor in MC38 cells. Table S1 provides the primer information used in this article.

Data availability

Qualified RNA samples were used for RNA-seq and data analysis (Novogene). Data analysis was performed using R software (R Foundation for Statistical Computing). RNA-seq data generated in this paper, underlying Figs. 1 and 3, have been deposited at the Gene Expression Omnibus (accession numbers GSE236339 and GSE236345).

In Fig. 6, D and E, we used the GEO2R built in the GEO database to compare two groups of samples (GSE225767) to identify genes that are differentially expressed across responder and non-responder in PDAC patients.

Other data can be found in the paper or online supplemental material.

Acknowledgments

We would like to thank Dr. Liufu Deng for sharing critical cell lines.

This study was supported by grants from the National Natural Science Foundation of China (no. 32170909 to W. Li, no.



82271840 to N. Miao, and no. 82003229 to F. Xia) and the Shanghai Municipal Health Commission (Youth Talents Program; no. 2022YQ077 to W. Li and no. 20214Y0096 to D. Cao).

Author contributions: N. Miao: Formal analysis, Funding acquisition, Investigation, Validation, Writing—original draft, Writing—review & editing, D. Cao: Formal analysis, Funding acquisition, Investigation, Validation, Writing—original draft, Writing—review & editing, J. Jin: Methodology, Writing—original draft, Writing—review & editing, G. Ma: Investigation, Writing—review & editing, H. Yu: Methodology, J. Qu: Methodology, G. Li: Formal analysis, Investigation, C. Gao: Formal analysis, Investigation, D. Dong: Methodology, F. Xia: Funding acquisition, Resources, Supervision, Writing—review & editing, W. Li: Conceptualization, Data curation, Formal analysis, Funding acquisition, Investigation, Methodology, Project administration, Resources, Software, Supervision, Validation, Visualization, Writing—original draft, Writing—review & editing.

Disclosures: D. Cao and W. Li reported a patent issued for a new target for overcoming radiotherapy resistance and its application. No other disclosures were reported.

Submitted: 22 August 2023 Revised: 20 May 2024 Accepted: 24 July 2024

References

- Arina, A., S.I. Gutiontov, and R.R. Weichselbaum. 2020. Radiotherapy and immunotherapy for cancer: From "systemic" to "multisite". Clin. Cancer Res. 26:2777–2782. https://doi.org/10.1158/1078-0432.CCR-19-2034
- Chen, X., A. Momin, S. Wanggou, X. Wang, H.K. Min, W. Dou, Z. Gong, J. Chan, W. Dong, J.J. Fan, et al. 2023. Mechanosensitive brain tumor cells construct blood-tumor barrier to mask chemosensitivity. *Neuron.* 111: 30–48.e14. https://doi.org/10.1016/j.neuron.2022.10.007
- Christensen, E., M. Pintilie, K.R. Evans, M. Lenarduzzi, C. Ménard, C.N. Catton, E.P. Diamandis, and R.G. Bristow. 2009. Longitudinal cytokine expression during IMRT for prostate cancer and acute treatment toxicity. Clin. Cancer Res. 15:5576–5583. https://doi.org/10.1158/1078-0432.CCR-09-0245
- Coste, B., J. Mathur, M. Schmidt, T.J. Earley, S. Ranade, M.J. Petrus, A.E. Dubin, and A. Patapoutian. 2010. Piezo1 and Piezo2 are essential components of distinct mechanically activated cation channels. *Science*. 330: 55–60. https://doi.org/10.1126/science.1193270
- Davis, M.J., S. Earley, Y.S. Li, and S. Chien. 2023. Vascular mechanotransduction. Physiol. Rev. 103:1247–1421. https://doi.org/10.1152/physrev.00053.2021
- Deng, L., H. Liang, M. Xu, X. Yang, B. Burnette, A. Arina, X.D. Li, H. Mauceri, M. Beckett, T. Darga, et al. 2014. STING-dependent cytosolic DNA sensing promotes radiation-induced type I interferon-dependent antitumor immunity in immunogenic tumors. *Immunity*. 41:843–852. https://doi.org/10.1016/j.immuni.2014.10.019
- Farrar, M.A., and R.D. Schreiber. 1993. The molecular cell biology of interferon-gamma and its receptor. Annu. Rev. Immunol. 11:571-611. https://doi.org/10.1146/annurev.iy.11.040193.003035
- Fiore, P.F., S. Di Matteo, N. Tumino, F.R. Mariotti, G. Pietra, S. Ottonello, S. Negrini, B. Bottazzi, L. Moretta, E. Mortier, and B. Azzarone. 2020. Interleukin-15 and cancer: Some solved and many unsolved questions. J. Immunother. Cancer. 8:e001428. https://doi.org/10.1136/jitc-2020-001428
- Frisoli, M.L., K. Essien, and J.E. Harris. 2020. Vitiligo: Mechanisms of pathogenesis and treatment. Annu. Rev. Immunol. 38:621-648. https://doi.org/10.1146/annurev-immunol-100919-023531
- Gajewski, T.F., H. Schreiber, and Y.X. Fu. 2013. Innate and adaptive immune cells in the tumor microenvironment. *Nat. Immunol.* 14:1014–1022. https://doi.org/10.1038/ni.2703

- Gupta, A., H.C. Probst, V. Vuong, A. Landshammer, S. Muth, H. Yagita, R. Schwendener, M. Pruschy, A. Knuth, and M. van den Broek. 2012. Radiotherapy promotes tumor-specific effector CD8⁺ T cells via dendritic cell activation. J. Immunol. 189:558–566. https://doi.org/10.4049/jimmunol.1200563
- Han, C., Z. Liu, Y. Zhang, A. Shen, C. Dong, A. Zhang, C. Moore, Z. Ren, C. Lu, X. Cao, et al. 2020. Tumor cells suppress radiation-induced immunity by hijacking caspase 9 signaling. *Nat. Immunol.* 21:546–554. https://doi.org/10.1038/s41590-020-0641-5
- Herrera, F.G., J. Bourhis, and G. Coukos. 2017. Radiotherapy combination opportunities leveraging immunity for the next oncology practice. *CA Cancer J. Clin.* 67:65–85. https://doi.org/10.3322/caac.21358
- Horiuchi, M., W. Hayashida, M. Akishita, S. Yamada, J.Y. Lehtonen, K. Tamura, L. Daviet, Y.E. Chen, M. Hamai, T.X. Cui, et al. 2000. Interferongamma induces AT(2) receptor expression in fibroblasts by Jak/STAT pathway and interferon regulatory factor-1. Circ. Res. 86:233-240. https://doi.org/10.1161/01.RES.86.2.233
- Ivashkiv, L.B. 2018. IFNγ: Signalling, epigenetics and roles in immunity, metabolism, disease and cancer immunotherapy. Nat. Rev. Immunol. 18: 545–558. https://doi.org/10.1038/s41577-018-0029-z
- Jin, P., L.Y. Jan, and Y.N. Jan. 2020. Mechanosensitive ion channels: Structural features relevant to mechanotransduction mechanisms. Annu. Rev. Neurosci. 43:207-229. https://doi.org/10.1146/annurev-neuro-070918-050509
- Kalbasi, A., C. Komar, G.M. Tooker, M. Liu, J.W. Lee, W.L. Gladney, E. Ben-Josef, and G.L. Beatty. 2017. Tumor-derived CCL2 mediates resistance to radiotherapy in pancreatic ductal adenocarcinoma. Clin. Cancer Res. 23: 137-148. https://doi.org/10.1158/1078-0432.CCR-16-0870
- Klug, F., H. Prakash, P.E. Huber, T. Seibel, N. Bender, N. Halama, C. Pfirschke, R.H. Voss, C. Timke, L. Umansky, et al. 2013. Low-dose irradiation programs macrophage differentiation to an iNOS⁺/M1 phenotype that orchestrates effective T cell immunotherapy. Cancer Cell. 24:589-602. https://doi.org/10.1016/j.ccr.2013.09.014
- Lang, X., M.D. Green, W. Wang, J. Yu, J.E. Choi, L. Jiang, P. Liao, J. Zhou, Q. Zhang, A. Dow, et al. 2019. Radiotherapy and immunotherapy promote tumoral lipid oxidation and ferroptosis via synergistic repression of SLC7A11. Cancer Discov. 9:1673–1685. https://doi.org/10.1158/2159-8290.CD-19-0338
- Lee, Y., S.L. Auh, Y. Wang, B. Burnette, Y. Wang, Y. Meng, M. Beckett, R. Sharma, R. Chin, T. Tu, et al. 2009. Therapeutic effects of ablative radiation on local tumor require CD8⁺ T cells: Changing strategies for cancer treatment. *Blood.* 114:589–595. https://doi.org/10.1182/blood-2009-02-206870
- Li, W., L. Lu, J. Lu, X. Wang, C. Yang, J. Jin, L. Wu, X. Hong, F. Li, D. Cao, et al. 2020. cGAS-STING-mediated DNA sensing maintains CD8⁺ T cell stemness and promotes antitumor T cell therapy. Sci. Transl. Med. 12: eaay9013. https://doi.org/10.1126/scitranslmed.aay9013
- Liang, H., L. Deng, Y. Hou, X. Meng, X. Huang, E. Rao, W. Zheng, H. Mauceri, M. Mack, M. Xu, et al. 2017. Host STING-dependent MDSC mobilization drives extrinsic radiation resistance. *Nat. Commun.* 8:1736. https://doi.org/10.1038/s41467-017-01566-5
- Liu, L., T. Gong, W. Tao, B. Lin, C. Li, X. Zheng, S. Zhu, W. Jiang, and R. Zhou. 2019. Commensal viruses maintain intestinal intraepithelial lymphocytes via noncanonical RIG-I signaling. *Nat. Immunol.* 20:1681–1691. https://doi.org/10.1038/s41590-019-0513-z
- Liu, X., Y. Jia, Z. Wang, Z. Zhang, and W. Fu. 2022. A pan-cancer analysis reveals the genetic alterations and immunotherapy of Piezo2 in human cancer. Front. Genet. 13:918977. https://doi.org/10.3389/fgene.2022 .918977
- Lou, W., J. Liu, B. Ding, L. Jin, L. Xu, X. Li, J. Chen, and W. Fan. 2019. Five miRNAs-mediated PIEZO2 downregulation, accompanied with activation of Hedgehog signaling pathway, predicts poor prognosis of breast cancer. Aging. 11:2628–2652. https://doi.org/10.18632/aging.101934
- Ma, S., M.A. Caligiuri, and J. Yu. 2022. Harnessing IL-15 signaling to potentiate NK cell-mediated cancer immunotherapy. Trends Immunol. 43: 833–847. https://doi.org/10.1016/j.it.2022.08.004
- McGillicuddy, F.C., E.H. Chiquoine, C.C. Hinkle, R.J. Kim, R. Shah, H.M. Roche, E.M. Smyth, and M.P. Reilly. 2009. Interferon gamma attenuates insulin signaling, lipid storage, and differentiation in human adipocytes via activation of the JAK/STAT pathway. J. Biol. Chem. 284:31936–31944. https://doi.org/10.1074/jbc.M109.061655
- McHugh, B.J., R. Buttery, Y. Lad, S. Banks, C. Haslett, and T. Sethi. 2010. Integrin activation by Fam38A uses a novel mechanism of R-Ras targeting to the endoplasmic reticulum. J. Cell Sci. 123:51-61. https://doi.org/10.1242/jcs.056424



- McLaughlin, M., E.C. Patin, M. Pedersen, A. Wilkins, M.T. Dillon, A.A. Melcher, and K.J. Harrington. 2020. Inflammatory microenvironment remodelling by tumour cells after radiotherapy. *Nat. Rev. Cancer.* 20: 203–217. https://doi.org/10.1038/s41568-020-0246-1
- Mlecnik, B., G. Bindea, H.K. Angell, M.S. Sasso, A.C. Obenauf, T. Fredriksen, L. Lafontaine, A.M. Bilocq, A. Kirilovsky, M. Tosolini, et al. 2014. Functional network pipeline reveals genetic determinants associated with in situ lymphocyte proliferation and survival of cancer patients. Sci. Transl. Med. 6:228ra37. https://doi.org/10.1126/scitranslmed 3007240
- Mondini, M., P.L. Loyher, P. Hamon, M. Gerbé de Thoré, M. Laviron, K. Berthelot, C. Clémenson, B.L. Salomon, C. Combadière, E. Deutsch, and A. Boissonnas. 2019. CCR2-Dependent recruitment of tregs and monocytes following radiotherapy is associated with TNFα-mediated resistance. Cancer Immunol. Res. 7:376–387. https://doi.org/10.1158/2326-6066 CIR-18-0633
- Oelert, T., M. Papatriantafyllou, G. Pougialis, G.J. Hämmerling, B. Arnold, and T. Schüler. 2010. Irradiation and IL-15 promote loss of CD8 T-cell tolerance in response to lymphopenia. *Blood*. 115:2196–2202. https://doi.org/10.1182/blood-2009-06-227298
- Ogasawara, K., S. Hida, N. Azimi, Y. Tagaya, T. Sato, T. Yokochi-Fukuda, T.A. Waldmann, T. Taniguchi, and S. Taki. 1998. Requirement for IRF-1 in the microenvironment supporting development of natural killer cells. *Nature.* 391:700–703. https://doi.org/10.1038/35636
- Palata, O., N. Hradilova Podzimkova, E. Nedvedova, A. Umprecht, L. Sadilkova, L. Palova Jelinkova, R. Spisek, and I. Adkins. 2019. Radiotherapy in combination with cytokine treatment. Front. Oncol. 9:367. https://doi.org/10.3389/fonc.2019.00367
- Piper, M., M. Hoen, L.B. Darragh, M.W. Knitz, D. Nguyen, J. Gadwa, G. Durini, I. Karakoc, A. Grier, B. Neupert, et al. 2023. Simultaneous targeting of PD-1 and IL- $2R\beta\gamma$ with radiation therapy inhibits pancreatic cancer growth and metastasis. *Cancer Cell.* 41:950–969.e6. https://doi.org/10.1016/j.ccell.2023.04.001
- Prokhnevska, N., M.A. Cardenas, R.M. Valanparambil, E. Sobierajska, B.G. Barwick, C. Jansen, A. Reyes Moon, P. Gregorova, L. delBalzo, R. Greenwald, et al. 2023. CD8⁺ T cell activation in cancer comprises an initial activation phase in lymph nodes followed by effector differentiation within the tumor. *Immunity*. 56:107–124.e5. https://doi.org/10.1016/j.immuni.2022.12.002
- Propper, D.J., and F.R. Balkwill. 2022. Harnessing cytokines and chemokines for cancer therapy. *Nat. Rev. Clin. Oncol.* 19:237–253. https://doi.org/10.1038/s41571-021-00588-9

- Raeber, M.E., Y. Zurbuchen, D. Impellizzieri, and O. Boyman. 2018. The role of cytokines in T-cell memory in health and disease. *Immunol. Rev.* 283: 176–193. https://doi.org/10.1111/imr.12644
- Richard, A.J., and J.M. Stephens. 2011. Emerging roles of JAK-STAT signaling pathways in adipocytes. Trends Endocrinol. Metab. 22:325–332. https:// doi.org/10.1016/j.tem.2011.03.007
- Rodriguez-Ruiz, M.E., I. Rodriguez, S. Garasa, B. Barbes, J.L. Solorzano, J.L. Perez-Gracia, S. Labiano, M.F. Sanmamed, A. Azpilikueta, E. Bolaños, et al. 2016. Abscopal effects of radiotherapy are enhanced by combined immunostimulatory mAbs and are dependent on CD8 T cells and crosspriming. Cancer Res. 76:5994–6005. https://doi.org/10.1158/0008-5472.CAN-16-0549
- Satir, P., and S.T. Christensen. 2007. Overview of structure and function of mammalian cilia. *Annu. Rev. Physiol.* 69:377–400. https://doi.org/10.1146/annurev.physiol.69.040705.141236
- Shen, J., Z. Zou, J. Guo, Y. Cai, D. Xue, Y. Liang, W. Wang, H. Peng, and Y.X. Fu. 2022. An engineered concealed IL-15-R elicits tumor-specific CD8⁺ T cell responses through PD-1-cis delivery. J. Exp. Med. 219:219. https://doi.org/10.1084/jem.20220745
- Siddiqui, I., K. Schaeuble, V. Chennupati, S.A. Fuertes Marraco, S. Calderon-Copete, D. Pais Ferreira, S.J. Carmona, L. Scarpellino, D. Gfeller, S. Pradervand, et al. 2019. Intratumoral Tcf1*PD-1*CD8* T cells with stem-like properties promote tumor control in response to vaccination and checkpoint blockade immunotherapy. *Immunity*. 50:195–211.e10. https://doi.org/10.1016/j.immuni.2018.12.021
- Szczot, M., A.R. Nickolls, R.M. Lam, and A.T. Chesler. 2021. The form and function of PIEZO2. Annu. Rev. Biochem. 90:507-534. https://doi.org/10 .1146/annurev-biochem-081720-023244
- Waldmann, T.A., and Y. Tagaya. 1999. The multifaceted regulation of interleukin-15 expression and the role of this cytokine in NK cell differentiation and host response to intracellular pathogens. *Annu. Rev. Immunol.* 17:19–49. https://doi.org/10.1146/annurev.immunol.17.1.19
- Xue, D., E. Hsu, Y.X. Fu, and H. Peng. 2021. Next-generation cytokines for cancer immunotherapy. Antib. Ther. 4:123–133. https://doi.org/10.1093/ abt/tbab014
- Yang, Y., M. Wu, D. Cao, C. Yang, J. Jin, L. Wu, X. Hong, W. Li, L. Lu, J. Li, et al. 2021. ZBP1-MLKL necroptotic signaling potentiates radiation-induced antitumor immunity via intratumoral STING pathway activation. Sci. Adv. 7:eabf6290. https://doi.org/10.1126/sciadv.abf6290
- Yokota, S., O. Yoshida, L. Dou, A.V. Spadaro, K. Isse, M.A. Ross, D.B. Stolz, S. Kimura, Q. Du, A.J. Demetris, et al. 2015. IRF-1 promotes liver transplant ischemia/reperfusion injury via hepatocyte IL-15/IL-15Rα production. J. Immunol. 194:6045–6056. https://doi.org/10.4049/jimmunol.1402505



Supplemental material



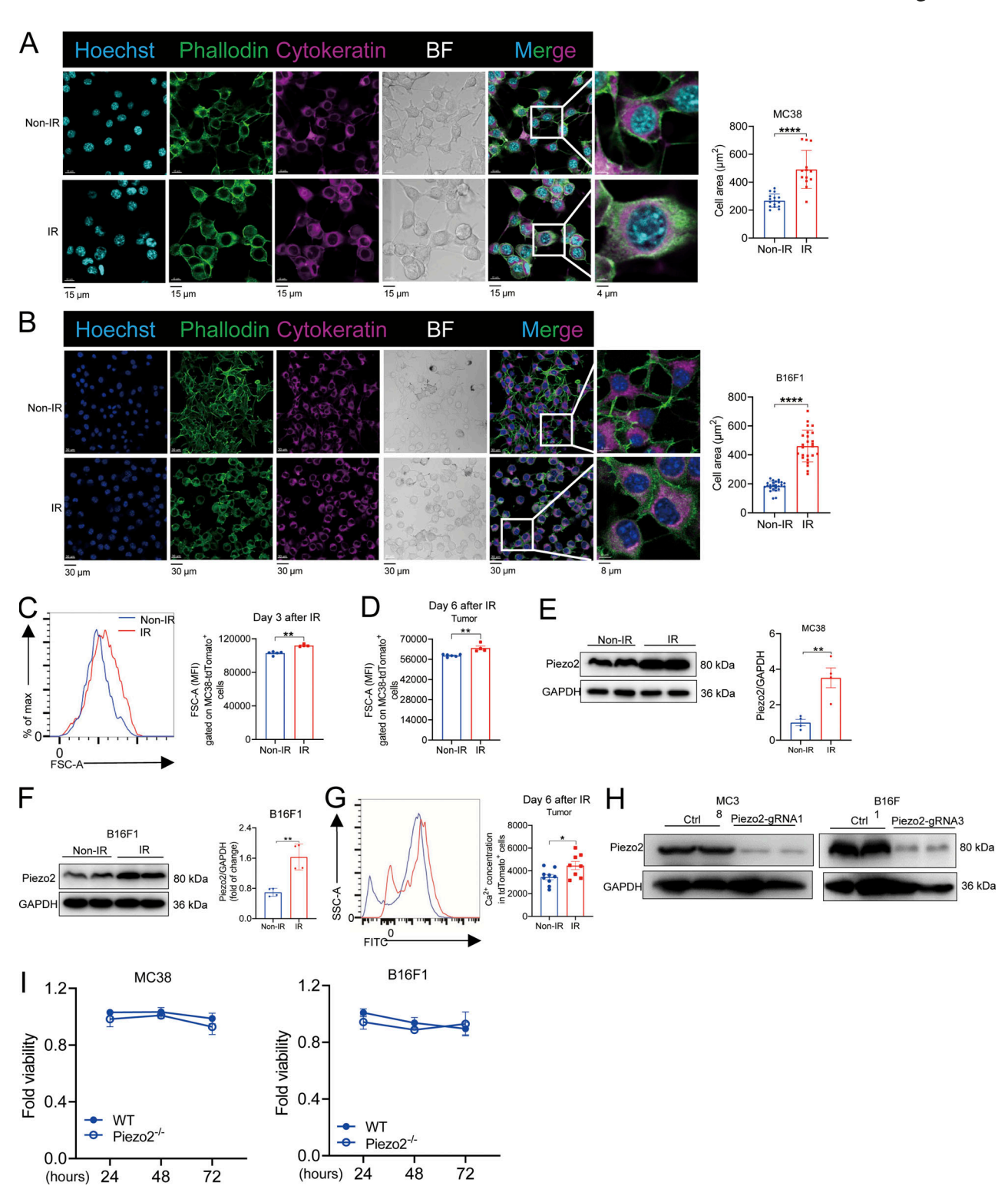


Figure S1. Cell size was changed after IR accompanied by the increase of Piezo2 expression and Ca²⁺ uptake. Related to Fig. 1. (A) The cytoskeleton staining in MC38 cells with or without radiation. Scale bar = 15 μ m. (B) The cytoskeleton staining in B16F1 cells with or without radiation. Scale bar = 30 μ m. (C and D) MFI of FSC-A tdTomato⁺ tumor cells from tumors on day 3 (C) and 6 (D) after IR were represented from three independent experiments (n = 4-6 mice per group). (E and F) The assessments of Piezo2 expression in MC38 (E) and B16F1 (F) tumor cells following radiation treatment were represented from three independent experiments. (G) Determination of Ca²⁺ concentration in tdTomato⁺ cells from irradiated tumors was shown from two independent experiments (n = 8-9 mice per group). (H) Determinations of Piezo2 expression in MC38 (E) and B16F1 (F) cells with or without gRNA were represented from three independent experiments. (I) Determinations of MC38 (left) and B16F1 (right) cell viability with or without Piezo2 by CCK-8 were shown from two independent experiments. Data were represented as means \pm SEM. The comparisons of two nonparametric datasets were calculated by Mann–Whitney U test (A and B). C–G were analyzed by unpaired Student's t test. *P < 0.05; **P < 0.01; ****P < 0.0001; ns, no significant difference. Source data are available for this figure: SourceData FS1.



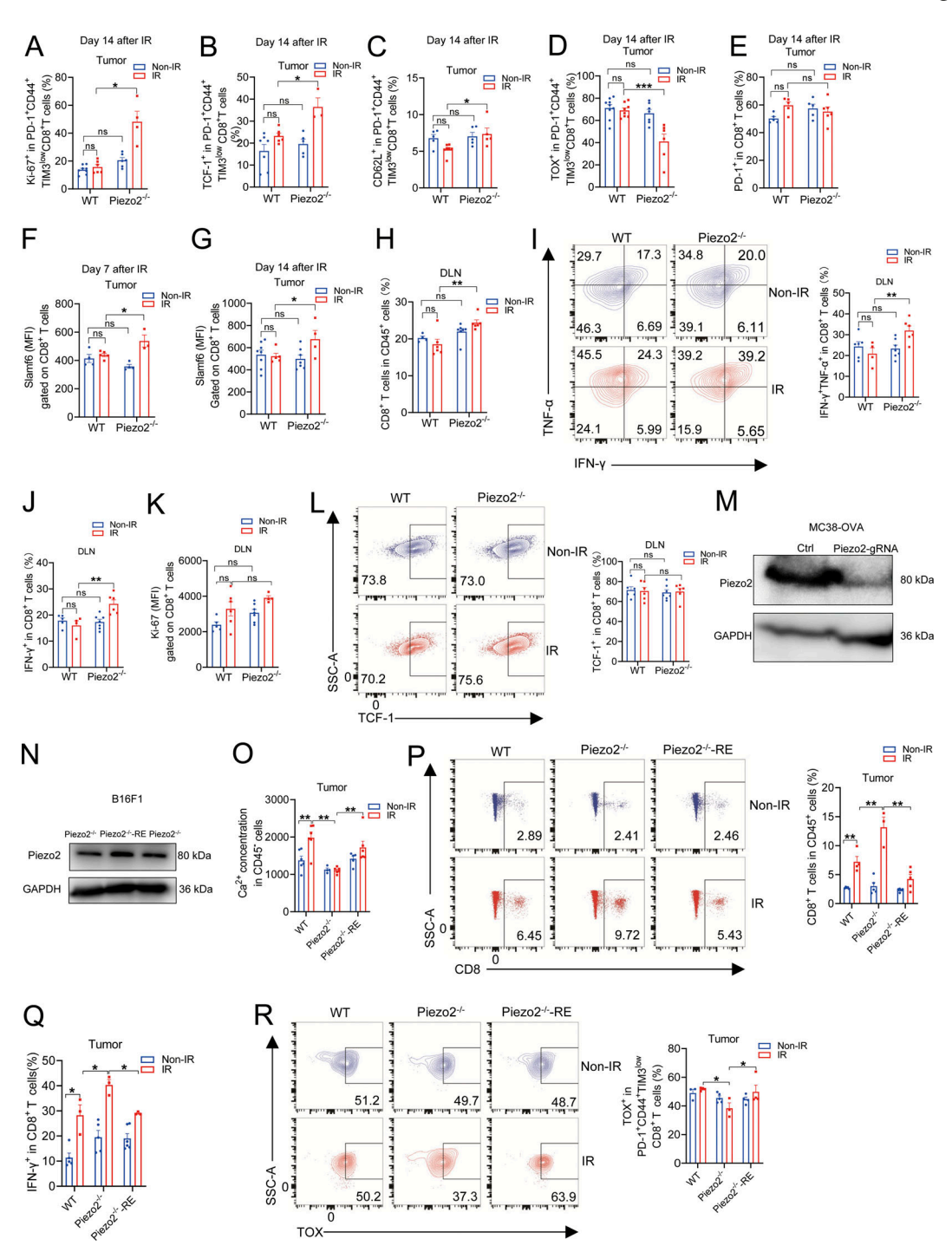


Figure S2. **Piezo2 deficiency in tumor cells affected CD8*** T cell infiltration and differentiation within irradiated tumors. Related to Fig. 2. **(A–D)** Quantifications of the percentage of Ki-67* (A), TCF-1* (B), CD62L* (C), and TOX* (D) in exhausted CD8* T cells from irradiated tumors on day 14 after IR were shown from two independent experiments (n = 3-9 mice per group). **(E)** Quantifications of PD-1* in CD8* T cells from irradiated tumors on day 14 after IR were shown from two independent experiments (n = 5-6 mice per group). **(F and G)** Quantifications of expression of Slamf6 on CD8* T cells from irradiated tumors on day 7 (F) and 14 (G) after IR were shown from two independent experiments (n = 3-8 mice per group). **(H–J)** The percentage of CD8* T cell (H), IFN- γ *TNF- α *CD8* T (I), and IFN- γ * CD8* T (J) cells in DLNs from tumor-bearing mice was represented from two independent experiments (n = 4-6 mice per group). **(K and L)** MFI summary of Ki-67 (K) and the proportion of TCF-1* (L) in CD8* T cells in DLNs were shown from two independent experiments (n = 4-7 mice per group). **(M)** The determination of Piezo2 expression in MC38-OVA cells with or without gRNAs was represented by two independent experiments. **(N)** The assessment of Piezo2 expression in Piezo2^{-/-} B16F1 with or without mPiezo2-CMV-Sport6 plasmid was shown from two independent experiments. **(O and P)** Ca²+ concentration measurement in CD45⁻ cells (O) and CD8* T cell infiltration (P) in CD45⁺ cells within irradiated WT, Piezo2^{-/-}, and Piezo2^{-/-}-RE tumors were shown from two independent experiments (n = 3-6 mice per group). **(Q and R)** The percentage of IFN- γ *CD8* T cells (Q) and TOX* among exhausted CD8* T cells (R) from irradiated WT, Piezo2^{-/-}, and Piezo2^{-/-}-RE tumors was represented from two independent experiments (n = 3-6 mice per group). Data were represented as means \pm SEM. Statistical analysis was performed by one-way ANOVA with multiple comparison tests. *P < 0.05; **P < 0.01, ns, no significant diff



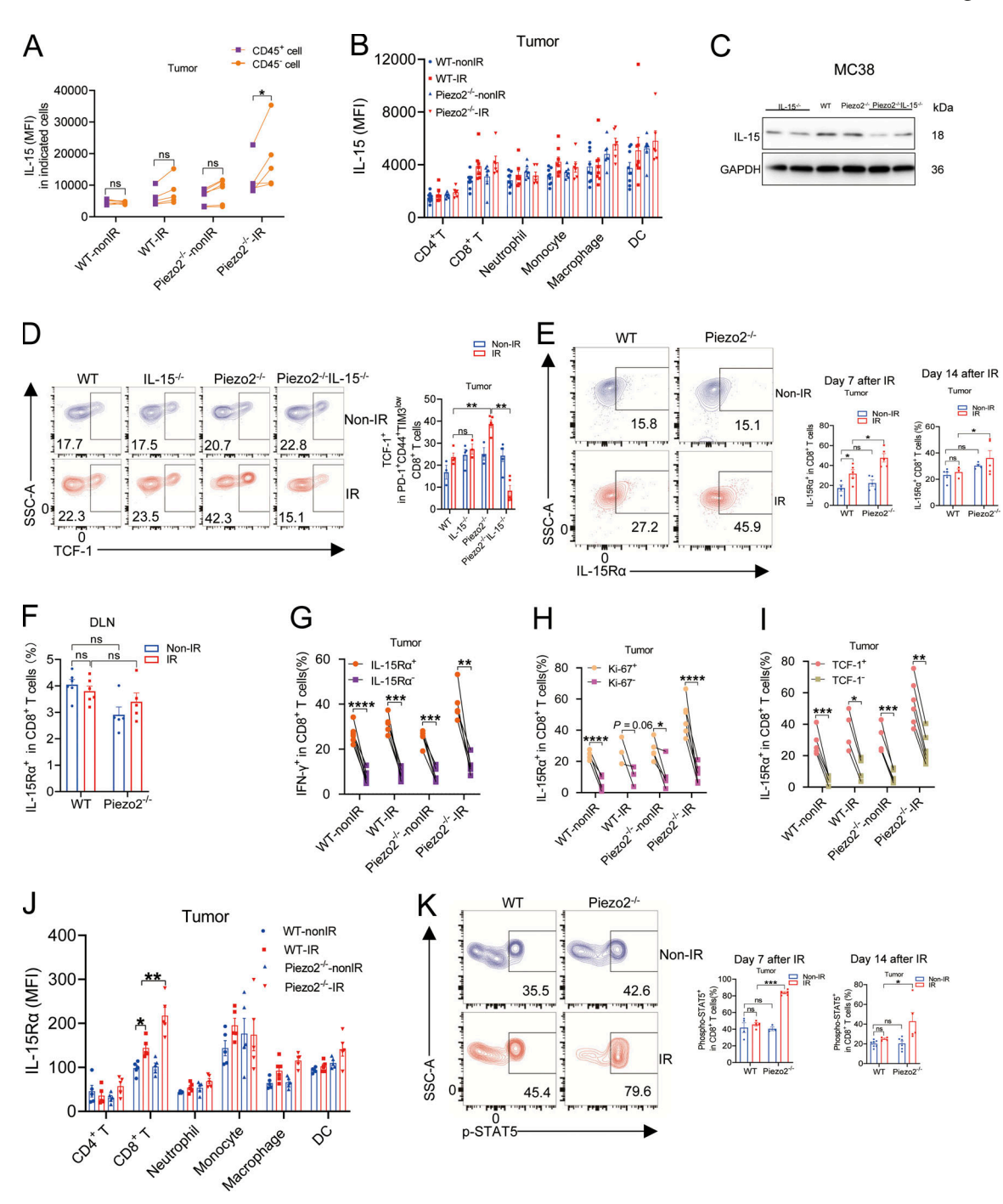


Figure S3. Tumor cell-derived IL-15 was required for tumor growth suppression enhancement and CD8* T cell regulation mediated by Piezo2 deficiency after IR treatment. Related to Fig. 3. (A) MFI summary of IL-15 expression in CD45* or CD45* cells in indicated MC38 tumors was represented from three independent experiments (n = 6-9 mice per group). (C) The knockdown efficiency of IL-15 expression in MC38 cells was shown in two independent experiments. (D) Representative data and quantification of the percentage of TCF-1* in exhausted CD8* T cells within irradiated WT, IL-15*-/-, Piezo2*-/-, and Piezo2*-/-IL-15*-/- tumors were shown from two independent experiments (n = 3-5 mice per group). (E) Representative data and quantification of the percentage of IL-15Ra* in CD8* T cells from WT and Piezo2*-/- MC38 tumors on day 7 and 14 after IR treatment were shown from three independent experiments (n = 4-5 mice per group). (F) Quantification of the percentage of IL-15Ra* in CD8* T cells from DLNs of WT and Piezo2*-/- MC38 tumor-established mice on day 5 after IR treatment was shown from two independent experiments (n = 5-6 mice per group). (G-I) The positive relevance of IL-15Ra with IFN- γ (G), Ki-67 (H), and TCF-1(I) in tumor-infiltrating CD8* T cells was shown by two independent experiments (n = 4-6 mice per group). (K) The expression of p-STAT5 in CD8* T cells from irradiated tumors on days 7 and 14 upon radiation treatment was represented by two independent experiments (n = 3-7 mice per group). Data were represented as means ± SEM. The comparisons of two datasets were calculated by paired Student's t test (A and G-I). Statistical analysis was performed by one-way ANOVA with multiple comparison tests (B, D-F, J, and K). *P < 0.05; **P < 0.01; ****P < 0.001; ****P < 0.0001, ns, no significant difference. Source data are available for this figure: SourceData FS3.



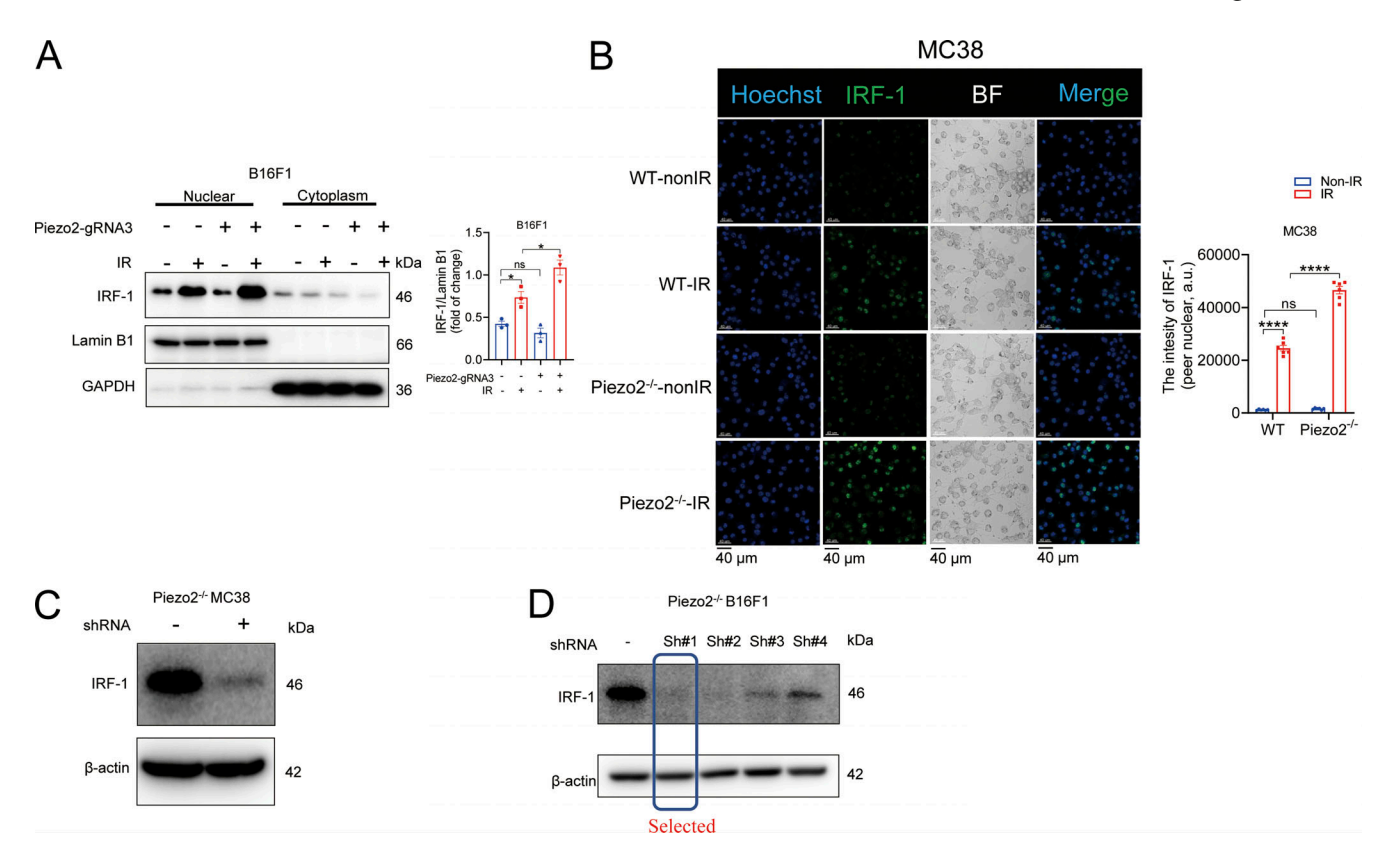


Figure S4. **IRF-1 was increased in irradiated cells and the KO efficiency determination for IRF-1 in Piezo2**^{-/-} **cells.** Related to Fig. 4. **(A)** The assessment of IRF-1 expression in nuclear and cytoplasm in irradiated B16F1 cells was represented from two independent experiments. **(B)** The determination of IRF-1 expression by immunofluorescence was shown by two independent experiments. Scale bar = 40 μm. **(C and D)** The KO efficiency determination of shRNA silencing for IRF-1 in Piezo2^{-/-} MC38 and Piezo2^{-/-} B16F1 cells was shown by two independent experiments. Data were represented as means ± SEM. Statistical analysis was performed by one-way ANOVA with multiple comparison tests. *P < 0.05; ****P < 0.0001; ns, no significant difference. Source data are available for this figure: SourceData FS4.

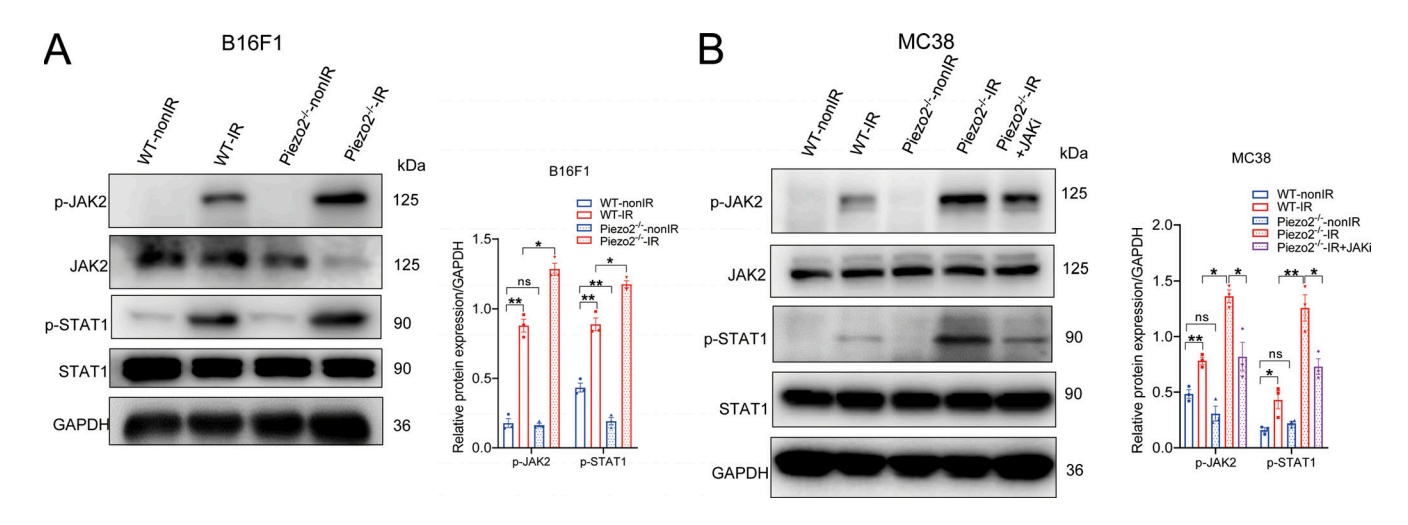


Figure S5. The measurement of JAK2/STAT1 activation in B16F1 cells and suppression of phosphor-JAK2/STAT1 expression by JAK inhibitor in MC38 cells. Related to Fig. 5. (A) The expression of p-JAK2 and -STAT1 expression in WT and Piezo2^{-/-} B16F1 cells with or without IR treatment was represented by three independent experiments. (B) The expression of p-JAK2 and -STAT1 in WT and Piezo2^{-/-} MC38 cells with or without JAK inhibitor following IR treatment was shown from three independent experiments. Data were represented as means ± SEM. Statistical analysis was performed by one-way ANOVA with multiple comparison tests. *P < 0.05; **P < 0.01; ns, no significant difference. Source data are available for this figure: SourceData FS5.

Provided online is Table S1. Table S1 provides the primer information used in this article.